NTNU – Trondheim
Norwegian University of
Science and Technology

Characterization of Underwater Acoustic Communication Channels

Statistical Characteristics of the Underwater
Multipath Channnels

Abraham Boayue

Master of Science in Communication Technology
Submission date: August 2013
Supervisor: Hefeng Dong, IET

Norwegian University of Science and Technology
Department of Electronics and Telecommunications

Master Thesis

August 26, 2013

Abstract

This master thesis aims at characterizing an underwater acoustic communication channel during the two day communication experiments conducted in the Trondheim Fjord by the NTNU Acoustic Group from the 17th and 18th of June 2013. During the experiments, part of the sea trials were devoted to the transmission of a pseudorandom binary sequence and a linear frequency modulation signal. The focus is put on the characterization of the statistical multipath channel in which the evolution of the channel temporal impulse response is examined together with the spreading and scattering functions. In addition, the channel power delay profile, Doppler power spectrum, delay spread, Doppler spread, coherence bandwidth, coherence time and the maximum excess delay of the power delay profile are presented in the form of figures and tables. Observation of the channel impulse response shows that the channel can be considered as a quasi-stationary channel and that the Doppler spread observed in the channel is mainly due to motion of the boat responsible for carrying the transmitter.

Acknowledgements

I would like to extend my gratitude and special appreciations to the following persons for making this project a success. Thanks to Prof. Hefeng Dong (Professor in Acoustic Remote Sensing) for allowing me undertake a project in a field that I was not so familier with from start. Thanks to my supervisor Postdoc Alexios-Georgios Korakas for his assistance in setting up the matlab platform and the correct estimation of the channel impulse response need for this project.

Contents

List of Figures

Chapter 1

Introduction

Underwater communication and networking has become very essential both for commercial and military purposes. The number of research conducted in this field has increased over the past few decades. The need to communicate between sensor nodes in sensor network requires the characterization of underwater acoustic channel. Because of the complexity of the underwater environment for communication, scientists have focused on different aspects of characterizing an underwater communication channel as in [1]. Each environment possesses a different characteristics that will affect the performance of a digital communication system [2]; therefore, a necessary step in accessing the performance of such systems is to be able to characterize an underwater communication channel based on measured data from the ocean.

The propagation of sound in the ocean is very complex and must be well understood. Due to reflections on the ocean's boundaries and refractions due to a depth varying sound speed, sound tends to propagate through multipath trajectories; the temporal variability of the ocean combined with the low sound speed in water may induce significant Doppler shifts. As a result the channel is affected by time and/or frequency dispersion. Generally, an underwater communication channel can be classified as a multipath fading channel, and should be characterized statistically.

A number of efforts made in the characterization of an underwater multipath communication channel include the work of P. van Walree [3] , P. van Walreeand and G. Bertolotto [4], and B. Borowski [2]. The work presented in this report focuses on characterizing the acoustic data collected during the two day communication experiments conducted in the Trondheim Fjord by the NTNU Acoustic Group from the 17th and 18th of June 2013 to produce results similar to [3] , [4] and [2]. This report is organized as follows: chapter 2 gives the necessary theory required for understanding and performing the simulations, chapter 3 describes the method of implementation starting with a brief description of the linear frequency modulation (LFM) signal in section 3.1 and a brief description of an m-sequence and its application to a binary modulation signal to produce a pseudorandom binary sequence (PRBS) in 3.2, chapter 4 presents the results of simulating a single channel with a PRBS signal for three different lengths and for an LFM signal, chapter 5 gives the conclusion, chapter 6 gives the bibliography and, finally, appendix A gives the matlab codes for producing most of the plots in the report and appendix B gives some reference plots to help aid the results obtained in chapter 4.

Chapter 2

Statistical Multipath Channel Characteristics

2.1 Multipath fading of the Wireless Channel

When a signal leaves the transmitting antenna, it can take a number of many different paths through a multipath communication channel to get to the receiver [5], and as a result, the transmitted signal components are scattered, reflected, diffracted, etc. by artificial or natural structures before reaching the receiver. If the transmitted signal is represented as i [6] and [7]:

$$\begin{aligned} s(t) &= Re\left[u(t)e^{j2\pi f_c t}\right] \\ &= Re\left[u(t)\right]\cos(2\pi f_c t) - Im\left[u(t)\right]\sin(2\pi f_c t), \end{aligned} \tag{2.1}$$

where $u(t)$ is the complex envelope and f_c is the carrier frequency, then the received signal at the receiver may be represented as the sum of the delayed components as:

$$\begin{aligned} r(t) =& \sum_{i=0}^{N(t)} \alpha_i(t) e^{\phi_{D_i}(t)} s(t - \tau_i(t)) \\ =& Re\left\{ \left[\sum_{i=0}^{N(t)} \alpha_i(t) u(t - \tau_i(t)) e^{-j2\pi\tau_i(t)} \right] e^{j2\phi f_c t} \right\} \end{aligned} \tag{2.2}$$

where $\phi_{D_i(t)}$ is the Doppler phase shift and amplitude $\alpha_i(t)$ and $\phi_i(t)$ is the associated phase of the ith signal component given by:

$$\phi_i(t) = 2\pi f_c \tau_i(t) - \phi_{D_i}(t) \tag{2.3}$$

Equation 2.2 shows that the received signal is obtained as the convolution between the time-variant multipath channel's impulse response and the transmitted signal if the channel's response is taken as:

$$C(\tau;t) = \sum_{i=0}^{N(t)} \alpha_i(t) e^{\phi_{D_i}(t)} \delta(t - \tau_i(t)) \tag{2.4}$$

Equation 2.2 can be manipulated to give:

$$\begin{aligned} r(t) &= r_I(t)\cos(2\pi f_c t) - r_Q(t)\sin(2\pi f_c t) \\ &= a\cos(2\pi f_c t + \phi(t)) \end{aligned} \tag{2.5}$$

where $r_I(t)$ and $r_Q(t)$ are the in-phase and quadrature signal components and a and $\phi(t)$ are the amplitude and phase of the received signal. The expressions for these components are given by:

$$r_I(t) = Re\left[\sum_{i=0}^{N(t)} \alpha_i(t) u(t - \tau_i(t)) e^{\phi_i(t)}\right] \tag{2.6}$$

$$r_Q(t) = Im\left[\sum_{i=0}^{N(t)} \alpha_i(t) u(t - \tau_i(t)) e^{\phi_i(t)}\right] \tag{2.7}$$

$$a = \sqrt{r_I^2(t) + r_Q^2(t)} \tag{2.8}$$

$$\phi(t) = \tan\left(\frac{r_Q(t)}{r_I(t)}\right)^{-1} \tag{2.9}$$

According to [5] and [6], if the locations of the structures in the signal's paths are completely random, one can assume the phase term, $\phi_i(t)$ will be uniformly distributed in the range $(0, 2\pi)$. For large valves of the order of the multipath, N, the amplitudes, $s_I(t)$ and $s_Q(t)$ will be independently, identically Gaussian distributed, and the envelope a will have a Rayleigh distribution as:

$$f(a) = \frac{a}{\sigma^2} e^{-\frac{a^2}{2\sigma^2}} U(a), \tag{2.10}$$

where σ^2 is the variance of either $r_I(t)$ or $r_Q(t)$, and $U(.)$ is the unit step function. Under this condition, the average power of the signal will have an exponential distribution given by:

$$f(p) = \frac{1}{2\sigma^2} e^{-\frac{p^2}{2\sigma^2}} U(p) \tag{2.11}$$

2.1.1 Multipath Channel Model for Time-Variant Channels

The complex-valued function given in equation 2.2 can be thought of as the response of the channel to the complex exponential function, $\exp(2\pi f_c t)$. The r.m.f (root-mean-square) spectral width of the channel, $C(\tau;t)$ is called the Doppler spread of the channel and is denoted as B_d; which is a measure of how rapidly the channel is changing with time. A small value of the Doppler spread results in a slowly varying of the channel with time, while a large value gives rise to a rapidly time varying channel.

2.1.2 The Tapped Delay Line Channel Model

A general model for a time-variant multipath channel is illustrated in Figure 2.1 taken from [8]. The channel model consists of a tapped delay line with uniformly spaced taps. The tap spacing between adjacent taps is 1/W, where W is the bandwidth of the signal transmitted through the channel. The taps coefficients of the channel are given by:

$$\begin{aligned} C_n(t) =& c_r(t) + jc_i(t) \\ =& \alpha_n(t)e^{j\phi_n(t)}, \end{aligned} \tag{2.12}$$

where $\alpha_n(t)$ is an attenuation factor and $\phi_n(t)$ is a phase shift. The coefficients, $c_r(t)$ and $c_i(t)$ are usually modeled as complex-valued Gaussian processes. The length of the delay line corresponds to the amount of time dispersion in the multipath channel, which is usually called the multipath delay spread. The multipath spread is denoted as $Tm = L/W$, where L represents the maximum number of possible multipath signal components.

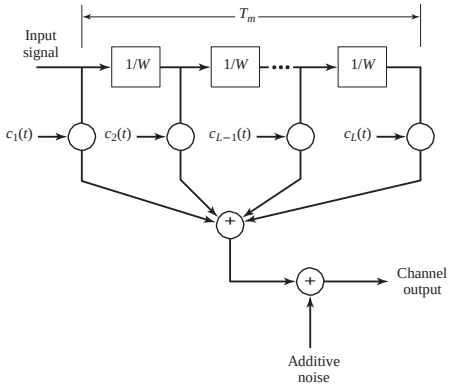

Figure 2.1: Model for time-variant multipath channel

2.1.3 Rayleigh and Ricean Fading Models

According to equation 2.12, if the coefficients of the tapped delay line channel model is treated as a complex-valued Gaussian process, then each of the coefficients may be expressed as:

$$C(t) = \alpha(t)e^{j\phi(t)}, \tag{2.13}$$

where the amplitude and phase are given by:

$$\alpha(t) = \sqrt{c_r^2(t) + c_I^2(t)} \tag{2.14}$$

$$\phi(t) = \tan^{-1}\left(\frac{c_I(t)}{c_r(t)}\right) \tag{2.15}$$

If the coefficients, $c_r(t)$ and $c_I(t)$ are zero mean Gaussian random variables, then the envelope has a Rayleigh distribution as given by equation 2.2 and the phase is uniformly distributed in the range of $(0, 2\pi)$. Thus, the channel is called a Rayleigh fading channel. On the other hand, if the coefficients, $c_r(t)$ and $c_I(t)$ are nonzero mean Gaussian random variables, then the amplitude $\alpha(t)$ will have a Ricean distribution as given by:

$$f(\alpha) = \frac{\alpha}{\sigma^2} e^{-(\alpha^2+s^2)/2\sigma^2} I_0\left(\frac{s\alpha}{\sigma^2}\right) \qquad a \geq 0, \tag{2.16}$$

where $2\sigma^2$ is the average power in the multipath components, $s^2 = \alpha_0^2$ is the power in the line of sight (LOS) component, and the function I_0 is the modified Bassel function of zeroth order. A typical plot of the Rayleigh and the Ricean fading channels is shown in Figure 2.2 obtained from an exercise in [5]. The plot was obtained from a total of 11 multipath components and using a random phase in generating the signal. The effect of the multipaths and random phase is clearly seen in the plots of the received powers; even in the absence of noise, the received power randomly varies.

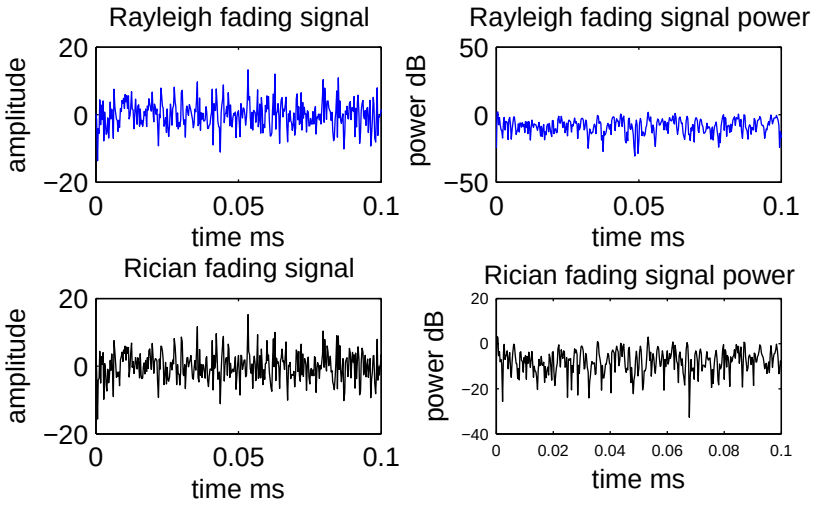

Figure 2.2: Rayleigh fading signal and power, and Ricean fading signal and power

2.1.4 Coherence Time and Coherence Bandwidth of the Channel

In addition to the delay spread T_m and the Doppler spread B_d, the coherence time and the coherence bandwidth are two other parameters that can be used to characterized fading, multipath channels. The coherence time is a measure of the time interval over which the channel characteristics will change very little and is given by:

$$T_c = \frac{1}{B_d} \tag{2.17}$$

Similarly, the coherence bandwidth is the bandwidth over which the channel characteristics (magnitude $\alpha(t)$ and phase ($\phi(t)$) are highly correlated. All frequency components of a signal within this bandwidth will fade simultaneously. This bandwidth is defined as the reciprocal of the delay time spread:

$$B_c = \frac{1}{T_m} \tag{2.18}$$

2.1.5 Multipath Channel Spread Factor

The product of the multipath spread and the Doppler spread ($T_m B_d$) is known as the channel spread factor. The channel is said to be underspread if $T_m B_d < 1$, and overspread if $T_m B_d > 1$. In general, the estimation of the carrier phase of the channel can be very difficult if the channel is overspread (rapid time variations $T_c << T_m$) due to either large multipath spread or either Doppler spread or both, and it can be estimated with good precision if the channel is underspread (slow time variations $T_c >> T_m$).

2.1.6 Dispersive Characteristics of the Channel

In addition to fluctuation of the received power as a result of fading, the shape of the pulse being transmitted is affected by the multipath channel. Because of the different paths taken by the transmitted signal components, the replicas of the pulse will arrive at the receiver at different times. If the pulses are not resolvable, the effect of the multipath is to produce a broadened pulse; this leads to intersymbol interference (ISI). Figure 2.3 (obtained from an exercise in [5]) shows the effect of ISI on the transmitted pulse, where a Gaussian pulse of width $\sigma_d = 14.14$ is being transmitted through a wireless channel. The dispersive behavior of the channel comes about in the sense that if a narrow pulse is transmitted through the channel, depending on the nature of the scattering, reflection, refraction or diffusion, the received multipath pulses may be spread out much more. Therefore, information arriving in the form of a finite size pulses will overlap and result in a broadened pulse as can be seen in Figure 2.3. The dispersive behavior of the channel can also be due to the Doppler effect if the receiver is traveling at a speed v. This motion will introduce a Doppler shift in the frequency of the received signal. The expression for the maximum Doppler frequency shift, f_D is given by:

$$f_{Dmax} = f_c \frac{v}{c}, \tag{2.19}$$

where c is the speed of sound in free space.

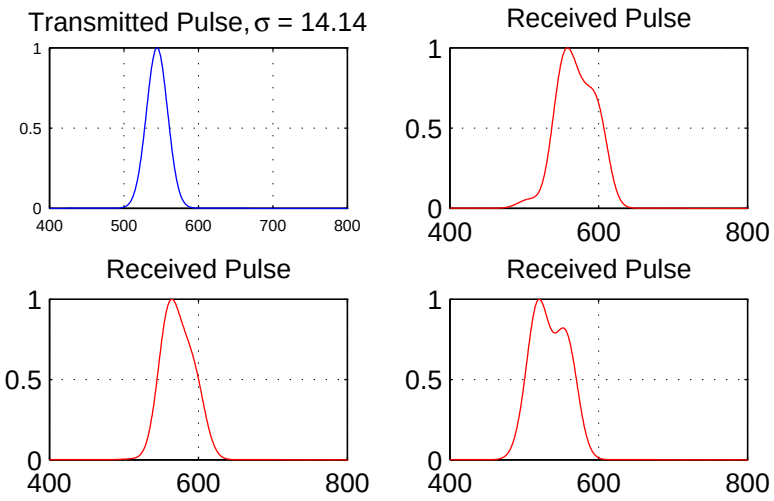

Figure 2.3: Simulation of a frequency selective channel, $\sigma_d = [14.14, 25.22, 24.26, 24.14]$

2.2 Characteristics of Underwater Acoustic Channels

Like communication on land, underwater communication channel can be regarded as time-varying frequency selective, spatially uncorrelated channel with additive colored Gaussian noise [9]. It is characterized by frequency dependent and range dependent absorption, which together with the multipath phenomenon results in fading. A few characteristics of the underwater acoustic channel is described in the next few subsections.

2.2.1 Doppler Shift

A relative motion of the receiver and or the transmitter or a moving medium can change the frequency of the sound waves propagating through the channel. The apparent change in the signal's carrier frequency and the time domain is known as Doppler shift. An expression for the Doppler frequency shift is given by:

$$f_D = f_c \frac{v + c}{c}, \tag{2.20}$$

where c is the speed of sound in free space,v speed of the observer and f_c the transmitted signal frequency known as the carrier frequency.

2.2.2 Multipath

In underwater acoustics the multipath effect is mainly caused by reflections from the sea floor and surface [9], [10]. The number of bounces determines the multipath spread. In addition, the channel consists of volume reflections such as plankton and fish. For a large enough range between the transmitter and receiver, the transmitted signal propagates to the receiver via various paths. The delay associated with each path depends on its geometry. The signals, while propagating, undergo successive reflections at the interfaces. Variations in the sound speed within the medium also deform the paths of the sound waves. Due to these processes, a given signal can therefore propagate from a source to a

receiver along several distinct paths corresponding to different directions and durations. The main direct signal arrives along with a series of echoes, the amplitudes which decrease with the number of reflections undergone. The process of signal taking many different paths to get to the receiver as a result of reflections is referred to as multipath. At high frequencies, for short signals, the multipath effect is observable in the time domain, with typical sequences of multiple echoes (see Figure 2.4, [10]). While for low-frequency stable signals, the contributions add together permanently; this creates a stable interference pattern, with strong variations in the field amplitude.

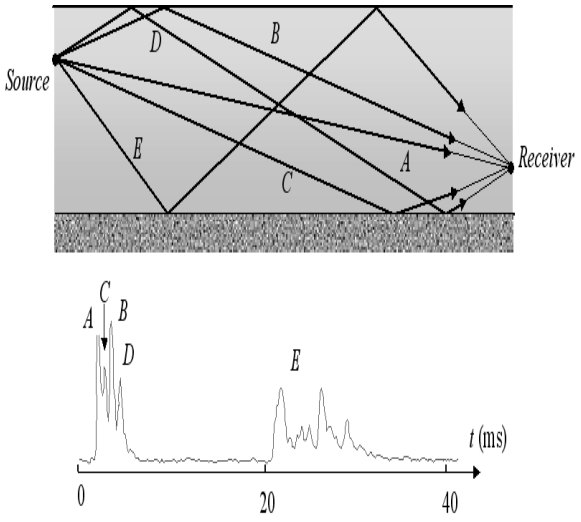

Figure 2.4: Top: Multipath trajectories in shallow-water configuration. (A) direct path, (B) surface reflection, (C) bottom reflection, (D) surface and bottom reflection, (E) bottom and surface reflection. Bottom: Multiple paths as visible in the envelope of a real time-domain signal. Note that the first group of 4 arrivals are very clearly distinguishable-spreads about 4 ms; a second group arrives 20 ms later with still a very significant intensity, and a more blurred time structure of the individual echoes tending to spread and to merge into a reverberation trail.

2.2.3 Doppler Spread

The Doppler spread B_d, expresses the spectral width spreading of the received signal. In shallow water the reflections from the water surface are the primary reason for the time-variance of the channel. The value of the Doppler spread depends on the waves height and frequency, wind speed, number of reflections from the sea surface and floor, and the nominal angle.

2.2.4 Delay-Spread and Doppler-Spread Functions

The theory of randomly time-variant linear channel was developed by Bello in his paper of 1963 [11]; he gave a full statistical characterization of the channel based on system functions and their correlation functions. He made use of the concept of a communication device consisting of an input and an output terminals; where the signal applied at the input may be characterized in either the time or frequency domain and similarly, the output signal coming out of the device may be characterized in either the time or frequency domain. Denoting $x(t)$ and $X(f)$ as the input time function and spectrum, and the corresponding out time function and spectrum as $y(t)$ and $Y(f)$, and using his approach and considering the underwater acoustic channel as a linear time variant filter (LTV), we can establish a mathematical relation between the input signal and the output signal. Since the underwater acoustic channel model to be discussed involves both delay and Doppler shifts, there exists a total of four expressions for the output signal; two for the time function and two for the frequency spectrum. The is because the channel will treat the signals differently depending on whether the delay operation or the Doppler-shift operation is applied at the input or output of the channel. For an input delay operator applied at the channel input, the convolution theorem gives the input-output relationship that exists between the input signal $x(t)$ and output signal $y(t)$ as:

$$y(t) = \int x(t-\tau)h(t,\tau)d\tau, \tag{2.21}$$

Equation 2.21 shows that the output of the channel is expressed as the integral of the delay elements; with the elements providing delays in the interval $(\tau, \tau + d\tau)$ and having a differential amplitude of $h(t,\tau)d\tau$. Therefore, the function $h(t,\tau)$ is called the Input Delay-Spread Function of the channel and may be thought of as the response of the channel at time t to a unit impulse input at time τ seconds in the past. Since a physical channel can not have an output before the input has arrived, $h(t,\tau)$ must vanish for $\tau < 0$. The second expression for the output signal is obtain by applying the delay operator at the output of the channel; the required expression is given by:

$$y(t) = \int x(t-\tau)g(t-\tau,\tau)d\tau, \tag{2.22}$$

where $g(t,\tau) = h(t+\tau,\tau)$ is referred to as the Output Delay-Spread-Function of the channel and may be thought of as the response τ seconds in the future to a unit impulse at time t. For the same requirement imposed on $h(t,\tau)$, $g(t,\tau)$ must vanish for $\tau < 0$.

The input-output relationship given by Equation 2.21 and 2.22 may be characterized in the frequency domain by employing the input and output Doppler-Spread Functions.If $H(f,\rho)$ is considered to be the dual function to $h(t,\tau)$, then the frequency domain representation of the output signal is given by:

$$Y(f) = \int X(f-\rho)H(f,\rho)d\rho, \tag{2.23}$$

where $H(f,\rho)$ is taken as the input Doppler-Spread Function and ρ as the Doppler shifted frequency variable. Similarly, the frequency domain representation to the output Doppler spread function is given by:

$$Y(f) = \int X(f-\rho)G(f,\rho)d\rho, \tag{2.24}$$

where $G(f,\rho)$ is taken as the output Doppler-Spread Function.

2.2.5 Delay-Doppler-Spread and Doppler-Delay-Spread Functions

Bello has demonstrated in [11] that any liner time-varying channel can be represented as a continuum of elements which simultaneously provide both a corresponding delay and Doppler shift. In his work, he classified the channel impulse response according to whether the delay operation or Doppler shift operation on the channel was at the input or the output. Because of the existence of the two operations in the channel model, only two possibilities were considered: input-delay output-Doppler-shift and input-Doppler-shift output-delay. Taking into account the former of the two possibilities, the input delay spread function $h(t,\tau)$ (i.e the time variance channel impulse response) can be expressed as the inverse Fourier transform of its Doppler spectrum $U(\tau,\rho)$ (holding τ as a fix parameter) given by:

$$h(t,\tau) = \int U(\tau,\rho)e^{j2\pi\rho t}d\rho, \tag{2.25}$$

Substituting this expression into Equation 2.21 gives:

$$y(t) = \int\int x(t-\tau)U(\tau,\rho)e^{j2\pi\rho t}d\rho d\tau, \tag{2.26}$$

Equation 2.26 shows that the output of the channel is expressed as the sum of the delay and then Doppler shifted elements; with the elements providing delays in the interval $(\tau,\tau+d\tau)$ and Doppler shifts in the interval $(\rho,\rho+d\tau)$ and having a differential amplitude of $U(\tau,\rho)d\rho d\tau$. Hence, the function $U(\tau,\rho)$ is called the Delay-Doppler-Spread Function of the channel.

To determine the Doppler-Delay-Spread function of the channel, we first express the input Doppler-Spread Function as the Fourier transform of $V(\rho,\tau)$ (holding ρ as a fixed parameter):

$$H(f,\rho) = \int V(\rho,\tau)e^{-j2\pi\tau f}d\tau, \tag{2.27}$$

Substituting this expression into Equation 2.23 gives:

$$Y(f) = \int\int X(f-\rho)V(\rho,\tau)e^{-j2\pi\tau f}d\tau d\rho, \tag{2.28}$$

Equation 2.28 shows that the output of the channel is expressed as the sum of the Doppler shifted and then Delay elements; with the elements providing Doppler shifts in the interval $(\rho,\rho+d\rho)$ and delays in the interval $(\tau,\tau+d\tau)$ and having a differential amplitude of $V(\rho,\tau)d\tau d\rho$. For this reason, the function $V(\rho,\tau)$ is called the Doppler-Delay-Spread Function of the channel. If the Fourier transform of both sides of Equation 2.26 is taken with respect to t, and the inverse Fourier transform of both sides of Equation 2.28 is taken with respect to f, we obtain the following two alternative expressions for the output signal of the channel in both time and frequency domains:

$$y(t) = \int\int x(t-\tau)e^{j2\pi(t-\tau)\rho}V(\rho,\tau)d\tau d\rho \tag{2.29}$$

$$Y(f) = \int\int X(f-\rho)e^{-j2\pi(f-\rho)\tau}U(\tau,\rho)d\tau d\rho \tag{2.30}$$

Equations 2.29 and 2.30 show that the Delay-Doppler-Spread Function $U(\tau, \rho)$ and the Doppler-Delay-Spread Function $V(\rho, \tau)$ are related through the following equation:

$$U(\tau, \rho) = e^{-j2\pi\rho\tau} V(\rho, \tau) \tag{2.31}$$

2.2.6 The Correlation Functions

In this section and the rest of the report, the channel is modelled as an input-delay output-Doppler shift channel. Hence, all mathematical expressions involving the channel impulse response are obtained in term of the input delay spread function $h(t, \tau)$ or equivalently, its inverse Fourier transform, the input Doppler spread function $U(\tau, \rho)$. The latter shall be called the spreading function as defined in [3]. The characteristics of a multipath channel can be defined through a number of useful correlation functions and power spectral density functions. According to [11], if the channel is randomly time-variant, the responses of the channel discussed in the last two sections become stochastic processes and a practical characterization of the channel is obtained in terms of correlation functions. It is customary to assume as in [1] and [6] that the fading statistics of many physical channels, including underwater acoustic channels to be approximately stationary for time intervals sufficiently long to make it meaningful to define a subclass of channels known as Wide-Sense Stationary (WSS) channels. If in addition, the channel response is further considered to be uncorrelated at the delays for $\tau_1 \neq \tau_2$, the channel can be called a Wide-Sense Stationary Uncorrelated Scattering Channel (WSSUSC). For simplicity, the channel impulse response can be modeled as in Equation 2.4. The channel autocorrelation function in the time domain can be represented as :

$$\begin{aligned} R_h(\tau_1, \tau_2, \Delta t) &= E\left[h^*(\tau_1, t) h(\tau_2, t + \Delta t\right] \\ &= R_h(\tau_1, \Delta t)\delta(\tau_2 - \tau_1) \\ &= R_h(\tau, \Delta t), \end{aligned} \tag{2.32}$$

Similarly, the channel autocorrelation function can be characterized in the frequency domain as :

$$\begin{aligned} R_h(f_1, f_2, \Delta t) &= E\left[h^*(f_1, t) h(f_2, t + \Delta t\right] \\ &= R_h(f_1, \Delta t)\delta(f_2 - f_1) \\ &= R_h(\Delta f, \Delta t) \end{aligned} \tag{2.33}$$

where the functions depend on the time variables τ_1 and τ_2 only through the time difference $\tau = \tau_2 - \tau_1$. The most important characteristics of the wideband channel, including the multipath intensity profile, coherence bandwidth, coherence time, and the Doppler power spectrum, are derived from the autocorrelation function $R_h(\tau, \Delta t)$. In addition to these, the scattering function $S(\tau, \rho)$, which completely characterizes the wideband channel if the WSSUS is assumed, can be defined; where ρ is the variable for the Doppler frequency shift in the frequency domain . By definition, the expression for the scattering function is given as the Fourier transform of the time autocorrelation function of the channel (Equation 2.32) or as the Fourier transform of the inverse Fourier transform of

the frequency autocorrelation function (Equation 2.33 see [6] and [4]):

$$\begin{aligned} S_h(\tau,\rho) &= \int R_h(\tau,\Delta t)e^{-j2\pi\rho\Delta t}d\Delta t \\ &= \int \left[\int h(\tau,t)h^*(\tau,t+\Delta t)dt\right] e^{-j2\pi\rho\Delta t}d\Delta t \\ &= \int \left[\int R_h(\Delta f,\Delta t)e^{j2\pi\tau\Delta f}d\Delta f\right] e^{-j2\pi\rho\Delta t}d\Delta t, \end{aligned} \tag{2.34}$$

Equation 2.34 shows that the time and frequency autocorrelaton functions, $R_h(\tau,\Delta t)$ and $R_h(\Delta f,\Delta t)$ form a Fourier transform pair. Letting Δt equals zero in both Equations 2.32 and 2.33, an expression for the multipath intensity profile can be obtained as :

$$P_h(\tau) = \int R_h(\Delta f)e^{j2\pi\tau\Delta f}d\Delta f, \tag{2.35}$$

where $R_h(\Delta f)$ is known as the spaced frequency correlation function of the channel. Similarly, to relate the Doppler effects to the time variations of the Doppler power spectrum, we let $A_c(\Delta f,\Delta t)$ denote the Fourier transform to the spectrum $S_c(\Delta f,\rho)$ and letting $\Delta f = 0$ we get an expression for the Doppler power spectrum:

$$S_h(\rho) = \int R_h(\Delta t)e^{-j2\pi\rho\Delta t}d\Delta t, \tag{2.36}$$

where $R_h(\Delta t)$ is known as the spaced time correlation function of the channel. The Fourier transform relationships among the correlation functions are summarized in [6] according to Figure 2.5.
Having set up a model for the time variant multipath channel and derived the autocorrelation function for it in both time and frequency domain, as well as equipped with the Fourier transform relationships that exist among the correlation functions, we devote a few sections in further characterization of the underwater acoustic channel.

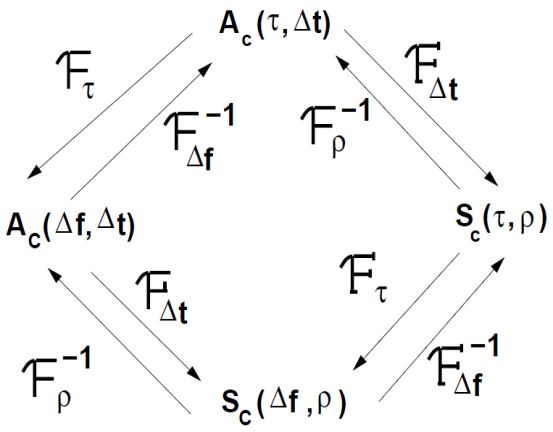

Figure 2.5: The Fourier transform relationships

2.2.7 Estimation of the Channel Correlation Functions and Parameters

It is more appropriate to have a discrete representation for the output signal of an underwater communication channel. Following the method of estimation outlined in [1] and

[18], the discrete representation to Equation 2.26 is given by :

$$y(n) = \sum_{(l,k)}^{L} x(n-l)U(l,k)e^{j2\pi k\Delta v n}, \tag{2.37}$$

where the L pairs (l,k) corresponds to L distinct scatterers at different delay and Doppler, and the channel is time dependent only through $e^{j2\pi k\Delta v n}$, Δv is the Doppler spacing, $x(n)$ is the input signal and $U(l,k)$ the delay Doppler spectrum or simply the spreading function as it is called in [3] and is defined as the Fourier transform of the channel impulse response, Equation 2.25. Hence, its discrete representation can be shown to be :

$$U(l,k) = \sum_{n=0}^{N-1} h(l,n)e^{j\frac{-2\pi nk}{N}}, \tag{2.38}$$

Assuming that the wide sense stationary uncorrelated scattering assumption (WSSUS) holds, the autocorrelation function can be defined as :

$$\begin{aligned} R_U(l,m;k,i) &= E[U_{l,k}U^*_{m,i}] \\ &= S(l,k)\delta(i-k)\delta(m-l), \end{aligned} \tag{2.39}$$

where $S(l,k)$ is the two dimensional power spectral density in delay and Doppler and is known as the channel scattering function, $R_U(l,m;k,i)$ is the autocorrelation function of the delay-Doppler-spread of the channel and δ is the Kronecker delta function. From a physical point of view, $U_{l,k}$ can be thought of as the complex gain of the received signal arriving at delay l and Doppler k. In the real world, the strength of the scatterer changes with time and therefore, the function $U_{l,k}$ is subject to change with time : $U_{l,k}(n)$. Hence, the channel is no longer a WSSUS channel. According to [1] the scattering function must be estimated in practice in addition to the WSSUS assumption. The scattering function can be estimated by transmitting a known signal; this signal must be chosen accordingly in order to obtain a good estimate of $S(l,k)$. The scattering function can be characterized in terms of ambiguity functions. The definitions of the signal ambiguity function and the cross-ambiguity function are given by :

$$\theta_0(l,k) = \left| \sum_{m=0}^{M-1} x(m)x^*(m-l)e^{-j2\pi k\Delta v m} \right|^2, \tag{2.40}$$

$$\theta(l,k) = \left| \sum_{m=0}^{M-1} x(m)y^*(m-l)e^{-j2\pi k\Delta v m} \right|^2, \tag{2.41}$$

where $x(m)y(m)$ is the complex baseband envelope of the transmitted and received signals. [1] and [18] have pointed out that the scattering function is related to the ambiguity function by showing that the expectation of the cross-ambiguity function is given by :

$$E[\theta(l,k)] = \sum_{(n,m)}^{L} \theta_0(l+n,k+m)S(n,m). \tag{2.42}$$

Equation 2.42 can be used to estimate the scattering function by selecting an appropriate source signal that will cause the ambiguity function to be a unit impulse in both delay and Doppler, i.e. the ambiguity function must equal :

$$\theta_0(l,k) = \delta(l)\delta(k) \tag{2.43}$$

An estimate of the delay power profile (multipath intensity profile) of the channel can be obtained by taking the average of the spreading function over all Doppler shifts :

$$P_u(l) = \sum_{k=0}^{N-1} |S(l,k)|^2 \tag{2.44}$$

The delay spread can be found by calculating the total delay of the delay power spectrum. Similarly, the Doppler power spectrum of the channel can be estimated by taking the average of the spreading function over all delays :

$$S_H(k) = \sum_{l=0}^{L-1} |S(l,k)|^2 \tag{2.45}$$

The Doppler spread B_d of the channel is found to be the bandwidth of the Doppler power spectrum $S_H(k)$. It is worth noting that Equations 2.44 and 2.45 may be valid for the spreading function $|U(l,k)|^2$ Equation 2.38; this is because in most instances the results obtained by using the scattering function can be approximated with that of the spreading function for most channels and hence, Equations 2.44 and 2.45 are valid for $|U(l,k)|^2$ since this is easier to obtain as shall be seen in Section 3.2. From the estimates of the delay power profile and the Doppler power spectrum, the spaced frequency correlation function and the spaced time correlation function can be estimated by taking the Fourier transform of Equation 2.44 and the inverse Fourier transform of Equation 2.45. Hence, the required expressions for these functions are :

$$R(\Delta f) = \sum_{l=0}^{L-1} P_u(l) e^{-j2\pi\Delta f l} \tag{2.46}$$

$$R(\Delta t) = \sum_{k=0}^{K-1} S_H(k) e^{j2\pi\Delta t k}, \tag{2.47}$$

Channel parameters

In section 1.1.4 the coherence time and coherence bandwidth of the channel were defined according to Equation 2.17 and 2.18, where the former was taken as the reciprocal of the Doppler spread and the latter as the reciprocal of the delay spread. These quantities can be obtained from the estimated correlation functions as defined in the preceding paragraphs. According to [6] the delay spread T_m is defined as the value over which the delay power profile is essentially non-zero, and the same is true for the Doppler spread B_d. Similarly, the coherence time T_c is taken as the value over which the spaced time correlation function is essentially non-zero, and the coherence bandwidth B_c is the value for which the spaced frequency correlation function is approximately zero for all $\Delta f > B_c$. The multipath channel can also be quantified in terms of the excess delay, average delay

spread $\bar{T_m}$ and the rms delay spread σ_{T_m}. The mathematical expressions for the $\bar{T_m}$ and $\sigma_{\bar{T_m}}$ in terms of the delay spread $R_h(\tau)$ are given by [6] as:

$$\bar{T_m} = \frac{\int_0^\infty \tau P_h(\tau) d\tau}{\int_0^\infty P_h(\tau) d\tau} \tag{2.48}$$

$$\sigma_{\bar{T_m}} = \frac{\int_0^\infty (\tau - T_m)^2 P_h(\tau) d\tau}{\int_0^\infty P_h(\tau) d\tau}, \tag{2.49}$$

If Equations 2.48 and 2.49 are defined in terms of the Doppler power spectrum, by [2] the resulting equations yield the corresponding expressions for the average delay spread and the rms delay spread in hertz:

$$f_{shift} = \frac{\int_0^\infty \rho S_h(\rho) d\rho}{\int_0^\infty S_h(\rho) d\rho} \tag{2.50}$$

$$\sigma_{f_{spread}} = \frac{\int_0^\infty (\rho - f_{shift})^2 P_h(\tau) d\tau}{\int_0^\infty S_h(\rho) d\rho}, \tag{2.51}$$

where f_{shift} and $\sigma_{f_{spread}}$ are the estimates of the maximum Doppler shift and the Doppler spread. Another parameter of interest of the channel is the maximum excess delay of the power delay profile. It is defined in [12] as the time delay during which the multipath energy falls to X-dB below the maximum value of the power delay profile. This quantity can be read from the plot of the power delay profile (see also [2]).

Chapter 3

Implementation

This chapter discusses some of the key points in characterizing an underwater communication channel using experimental data. The chapter aims at justifying that the ambiguity function method of estimating the channel scattering function is appropriate. The accuracy of the method is possible through a careful selection of the source signal. Hence, it is very useful to compute the ambiguity diagrams for various waveforms and determine which one of them have the desirable properties for the intended application [13]; two types of signals have been used to test the method. The signals are : linear frequency modulation (LFM) signal and a binary phase shift keying signal with the bit sequence generated from a maximum length sequence (m-sequence). A very good understanding of the ambiguity function is covered in [14] and [13]. A study of the ambiguity diagram can provide some insights about how different signal waveforms may be suitable for various communication purposes. The ambiguity function has the following mathematical properties :

$$|\theta_0(\tau,\rho)|^2_{max} = |\theta_0(0,0)|^2 = (2E)^2 \tag{3.1}$$

$$|\theta_0(-\tau,-\rho)|^2 = |\theta_0(\tau,\rho)|^2 \tag{3.2}$$

$$|\theta_0(\tau,0)|^2 = \left|\int x(t)x(t+\tau)dt\right|^2 \tag{3.3}$$

$$|\theta_0(0,\rho)|^2 = \left|\int x(t)^2 e^{j2\pi\rho t}dt\right|^2 \tag{3.4}$$

$$\int\int |\theta_0(\tau,0)|^2 \, d\tau d\rho = (2E)^2 \tag{3.5}$$

Equation 3.1 states that the maximum of the ambiguity function occurs at the origin, which is the output of the matched filter that is matched perfectly to the signal reflected from the target of interest; its value is equal to the square of two times the echo signal energy. The second equation is a symmetry equation. Equation 3.3 is just the portion of the ambiguity function on the time delay axis, which is the square of the autocorrelation function of the transmitted signal. Equation 3.4 describes the behaviour of the function along the frequency axis and is equal to the inverse Fourier transform of the square of the signal $x(t)$. Finally, Equation 3.5 gives the total volume under the ambiguity diagram, and is equal to $(2E)^2$.

3.1 The Linear frequency Modulation Signal (LFM)

An LFM signal is commoly referred to as a chirp signal and may be expressed as a cosine signal as in [15] and [16] :

$$x(t) = \cos(2\pi f_0 t + \pi k t^2), \tag{3.6}$$

where k is known as the chirp rate or the frequency slope defined as :

$$|k| = \frac{|f_1 - f_0|}{T} = \frac{B}{T}. \tag{3.7}$$

Equation 3.6 and 3.7 completely characterize the chirp signal by its start frequency f_0, stop frequency f_1 or bandwidth B and time duration T. The following plots in Figure 3.1 shows the results of a chirp signal simulated for a start frequency of $f_0 = 3500$ Hz, stop frequency of $f_1 = 4000$ Hz and a period of $T = 25$ ms. It is clear from these plots that the use of the LFM signal for estimating the scattering function will yield undesirable results; two reasons being that the output of the matched filter does not approximate an impulse along the Doppler axis, and the side lobes have very high values as opposed to the negligible side lobe criterion.

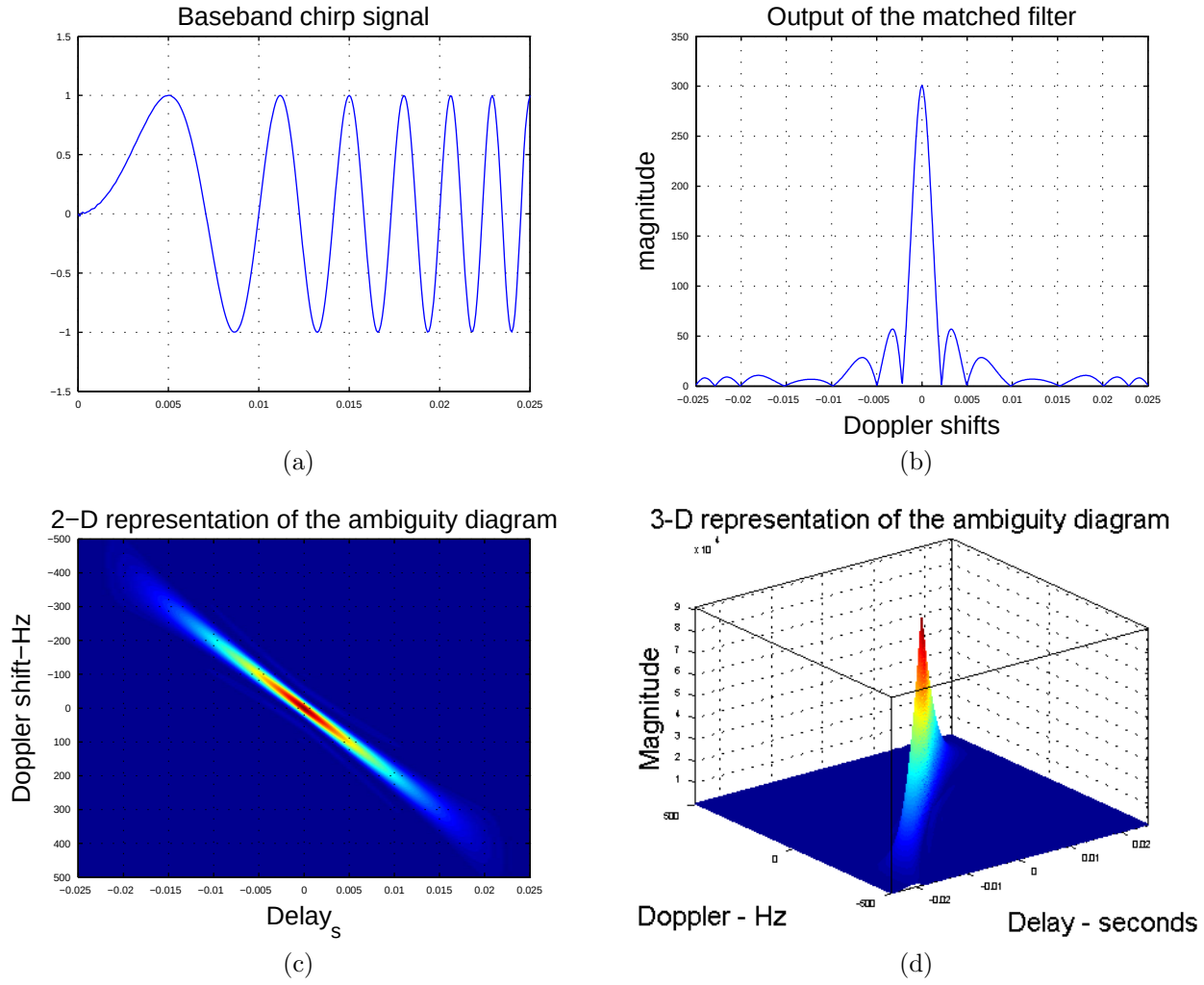

Figure 3.1: Testing the ambiguity function of a chirp signal: (a)Chirp signal(b)Matched filter output, (c) 2-D plot of the ambiguity function (d)3-D plot of the ambiguity function

3.2 Maximal Length Sequence

A maximal length sequence (MLS) is a periodic two-level signal that can be generated from a linear feedback shift register; it has a length of $N = 2^m - 1$, where m is the number of stages in the shift register and N is the period. A MLS is commonly called an m-sequence and can be generated by a polynomial $G(x)$ of degree m, where $G(x)$ is defined as :

$$G(x) = \sum_{i=0}^{m} a_i x^i, \tag{3.8}$$

where the a_is are the feedback taps that have values of either 0 or 1 depending on whether the feedback tap is connected or not. It should be noted that m-sequences are a special case of the output of a feedback shift register that will make every state transition of 2^m of an m-bit shift register with the exception of the all zero state. Hence, an m-sequence will only exist only if proper feedback taps are chosen. M-Sequences have a number of desirable properties that make them very useful in practice; because of their optimal noise-

like characteristics, they can be referred to as pseudo-noise or pseudo-random sequences. The most important property of an m-sequence is its desirably periodic autocorrelation function. If it is mapped to an analogue time varying signal, by mapping 0 to -1 and 1 to 1 or vice versa, then the resulting autocorrelation function for the resulting waveform will be unity for zero delay, and $1/N$ for any delay greater than one-bit, either positive or negative in time. The shape of the resulting autocorrelation function between +1 and -1 will be triangular and having a maximum at zero lag. Please see [17], [7] and [13] for a complete discussion of the m-sequence. The pseudo-random binary sequences used for testing the properties of the ambiguity function and broadcast during the experiment can be described according to [4] by :

$$x(t) = \cos(2\pi f_c t) \sum_{n=1}^{N} \sum_{m=1}^{M} C_m g(t - mT - nMT), \tag{3.9}$$

where $g(t)$ is a band-limited root raised cosine pulse given by :

$$g(t) = \frac{T^2 \cos(2\pi t/T)}{T^2 - 16t^2}, \tag{3.10}$$

where T denotes the bit duration and f_c the carrier frequency. In Equation 3.9, the summation creates a pseudo-random code of M bits with C_m taking on values of -1 or 1 depending on whether the transmitted bit was a zero or one. The following plots shown in Figure 3.2 illustrate an m-sequence generated by a simple feedback shift register having 9 stages corresponding to a period of 511; the autocorrelation function is seen to be a perfect Dirac signal except for the errors on both sides of the maximum value. A plot of the raised cosine pulse is also shown along with its modulated version at a carrier frequency of 1000 Hz.

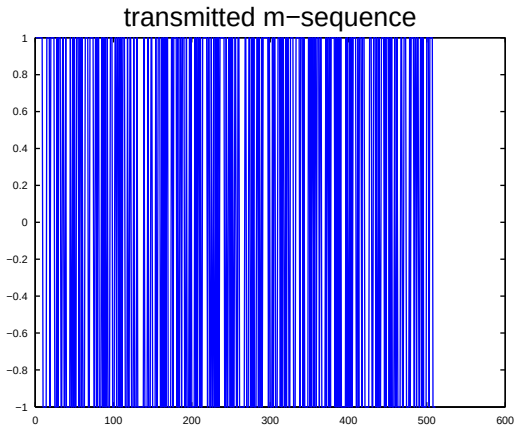

(a)

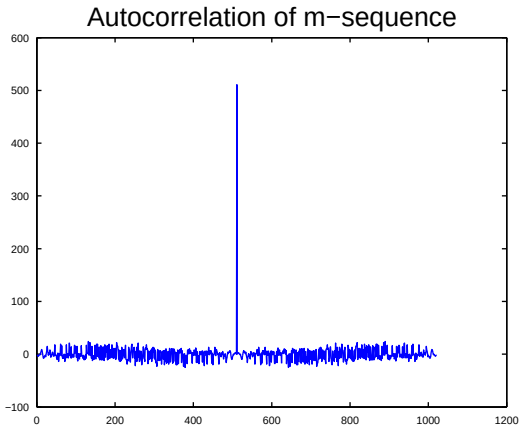

(b)

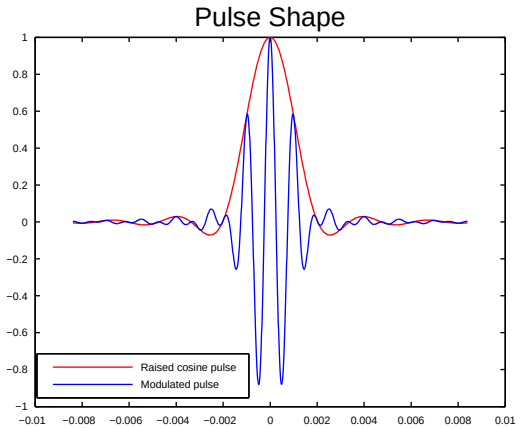

(c)

Figure 3.2: A plot showing : (a)M-sequence of period 511(b)The corresponding autocorrelation function, (c) The raised cosine pulse and its modulation at fc = 1000 Hz

The result of testing with pseudo-random binary sequences in estimating the channel scattering function seems promising as shown in Figure 3.3. The criterion that the signal ambiguity function be a Dirac in both the Doppler and time domains as proposed by Equation 2.43 is much satisfactory as can be seen in the plots of the 2-D and 3-D representations of the ambiguity diagrams. Comparing the two 2-D diagrams of the two signals (PRBS and LFM), it can be seen that they both have the same response at zero frequency shifts, and differ elsewhere. However, the PRBS signal has a high resolution in both delay and Doppler and suffers from clutter at Doppler shifts other than zero. On the other hand, the LFM signal has stronger response for Doppler shifted signals than the PRBS waveform. For this reason, LFM signals are known to be highly Doppler insensitive, but introduces a delay shift of $\Delta\tau = \frac{\rho T}{B}$. A phenomenon known as Delay-Doppler coupling. It is also clear from the plot that the LFM signal broaden for large frequency shifts.

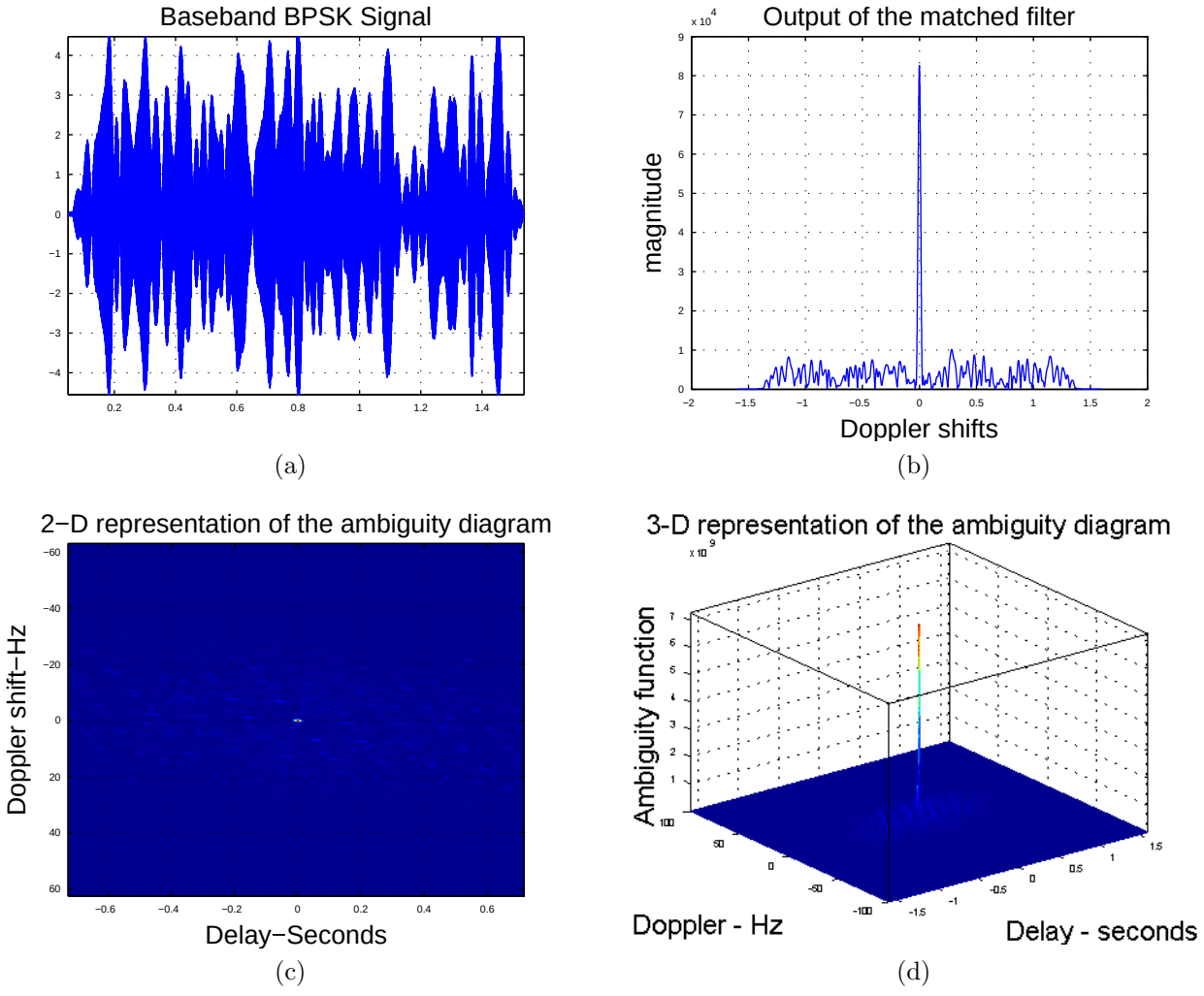

Figure 3.3: Testing the ambiguity function of a BPSK signal: (a)BPSK signal(b)Matched filter output, (c) 2-D plot of the ambiguity function (d) 3-D plot of the ambiguity function

Chapter 4

Simulations

This chapter presents the method and results of characterizing an underwater acoustic communication channel based on experimental data collected from the Trondheim Fjord. During the experiments, a total of 20 channels labelled 1 to 20 were measured by transmitting two types of signals, an LFM signal and a BPSK signal. Of the 20 channels measured, only one was chosen for the purpose of analysing the effects of characterizing the channel based on the two signals chosen. An overview of the experiments and the results of characterizing channel 4 is covered in the next subsection. The following references are relevant to understanding the results presented here, [3], [4] and [2].

4.1 Trondheim Fjord Experiments

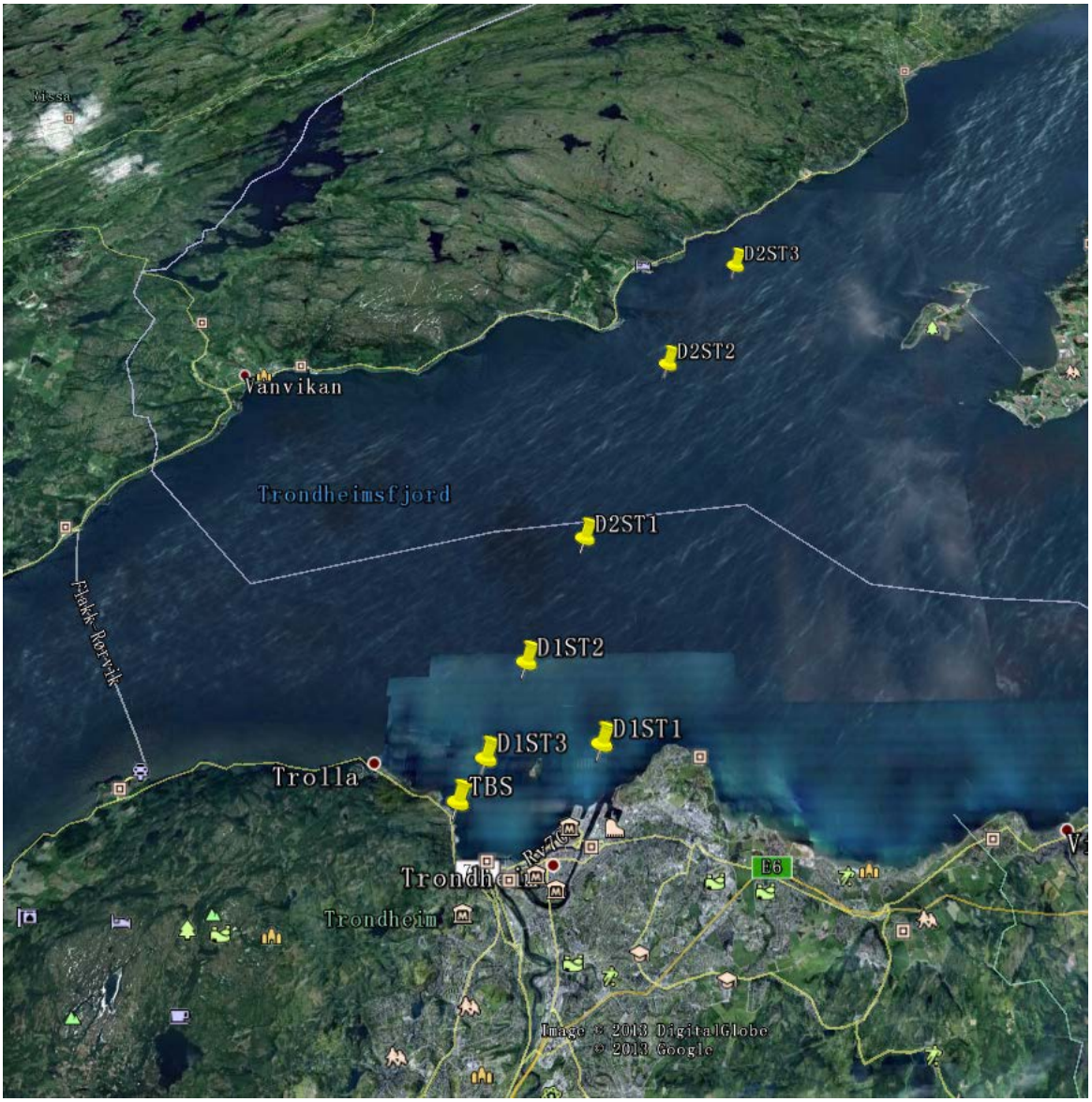

Figure 4.1: Experimental locations

The Trondheim Fjord experiments were carried out by the NTNU Acoustic Group from the 17th to 18th of June 2013. The purpose of the experiments was to broadcast signals of different wave forms and perform a measurement of the underwater communication channels to be analysed at the NTNU Acoustic lab. The data for the channels was collected from six different sits labeled as D1ST1 to D1ST3 and D2ST1 to D2ST3. The receiver was deployed at the Trondheim Biological Station (TBS) as shown in Figure 4.1. Two transducers were deployed on board the boat R/V Gunnerus from which the modulated acoustic waves were transmitted having center frequency of 12 kHz (high frequency) and 1 kHz (low frequency). During the experiment, both an m-sequence and LFM wave forms were transmitted; the receiving system was composed of a high sampling rate recorder, pre-amplifiers, filters, 1 vertical array with 8 elements and a cross array with 2 to 4 elements.Table 4.1 shows the GPS coordinates, distance and bearing from TBS, and source

depths for sound transmission during the two day experiments.

Day	No.	GPS coordinates	Distance and Bearing from TBS	source depth (m)
1	D1ST1	63° 27.2'N 63°24.7833'E	3.64 km 66.9°	20*
1	D1ST2	63°28.3166'N 10°22.5333'E	3.87 km 21. 12°	20*
1	D1ST3	63°27.0085'N 10°21.559'E	1.29 km 28. 84°	20*
2	D2ST1	63°30.1833'N 10°24.1166'E	7.53 km 20. 53°	20*
2	D2ST2	63°33.2181'N 10°26.7333'E	13.72 km 20. 98°	20*
2	D2ST3	63°35.2'N 10°29.1833'E	17.78 km 22. 72°	20*

* Source depths will depend on sound-speed profile and are subject to correction in case of low quality reception

Table 4.1: The GPS coordinates, distance and bearing from TBS, and source depths for sound transmission

The data analysed in this report was collected on Day 1 of the experiments from site D1ST3 and the results presented here were acquired from the transmission of an LFMs signal and a BPSK modulated signal as given in Equation 3.9. A few characteristics of the signals transmitted are shown in Table 4.2. In this report, the steps involved in analysing the data are as follows: Firstly, the passband transmitted signal was converted to an equivalent baseband signal to eliminate the dependency of the analysis on the carrier frequency, and then re-sampled so as to reduce the very high sampling frequency used during transmission; a similar analysis was performed on the received signal. Secondly, the received signal was matched filtered with the transmitted signal to obtain an estimate of the impulse response for each transmission. Thirdly, the estimated impulses were stacked against the transmission time to obtain the temporal impulse response of the channel. Finally, the temporal impulse response of the channel was used to obtain an estimate of the spreading and the scattering functions according to Equations 2.38and 2.34; based on these two equations, an estimate of both the power delay profile and the Doppler power spectrum were obtained according to Equations 2.44 and 2.45 .

Signal ID	PN8	PN9	PN10	LFMSig
Bandwidth (Hz)	7000	7000	7000	7000
Carrier Freq. (Hz)	10000	10000	10000	10000
Bit-rate Rb (s^{-1})	3500	3500	3500	3500
Sequence length (M)	255	511	1023	-
Sequence Duration MT(s)	0.073	0.146	0.292	-
Delay time resolution T(ms)	0.29	0.29	0.29	0.29
Doppler resolution R_D (m/s)	-	-	-	-

Table 4.2: Parameters of the transmitted signals

4.2 Results of Channel 4

This section presents the results of analysing channel 4 based on pseudo-random binary sequences (PRBS) as defined in Equation 3.9 and an LFM probe signal. The PRBS signal has been generated using m-sequences for three different lengths of sequences; see Table 4.2. The results obtained are shown in the form tables and figures :

- An estimate of the channel temporal impulse response
- The spreading function, $|U(l,k)|^2$ Eq. 2.38
- The scattering function, $|S(\tau,\rho)|^2$ Eq. 2.34
- The power delay profile, Eq 2.44 based on both $|U(l,k)|^2$ and $|S(\tau,\rho)|^2$
- The Doppler power spectrum, Eq 2.45 based on both $|U(l,k)|^2$ and $|S(\tau,\rho)|^2$
- Tables containing estimated values of the average delay spread, rms delay spread, maximum Doppler shifts, Doppler spread (all of these are based on Equations 2.48, 2.49, 2.50 and 2.51), coherence bandwidth, the coherence time and the maximum excess delay of the power delay profile; these are all read from their respective functions

Simulation results for a PRBS signal of length 255

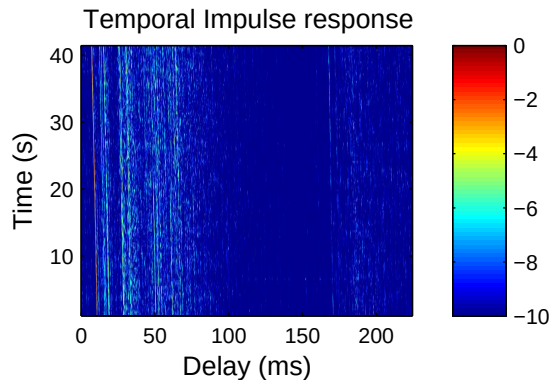

(a)

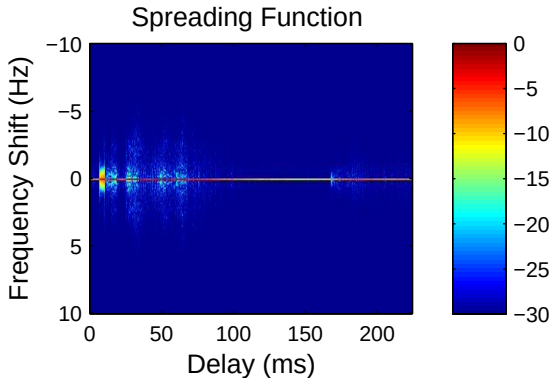

(b)

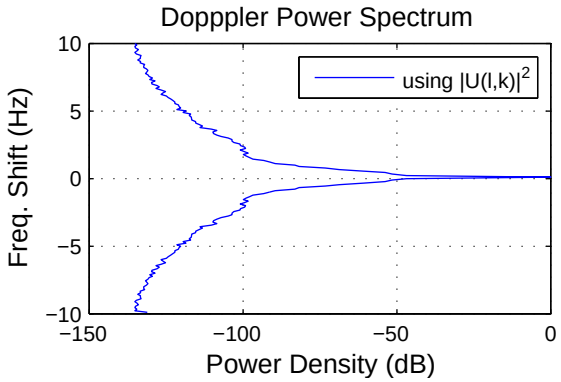

(c)

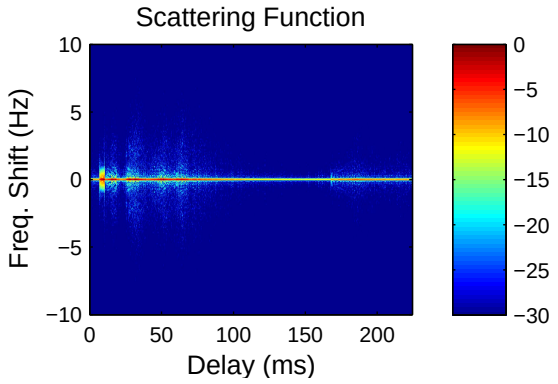

(d)

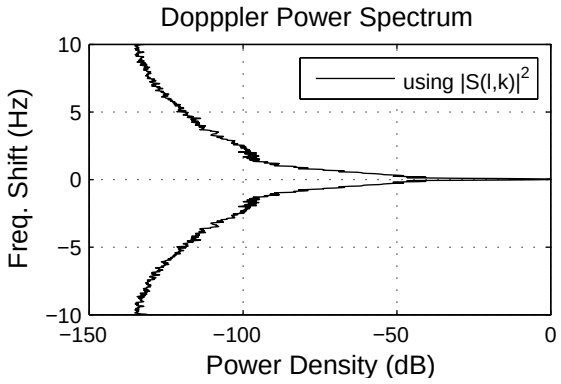

(e)

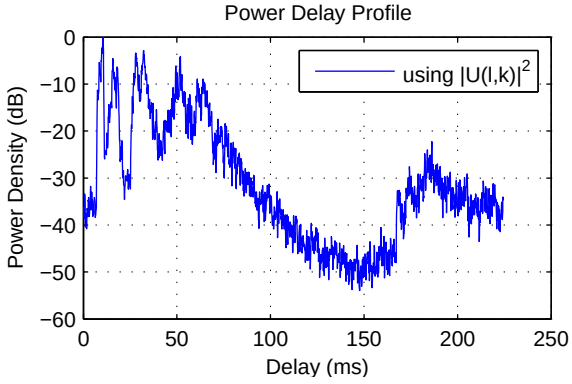

(f)

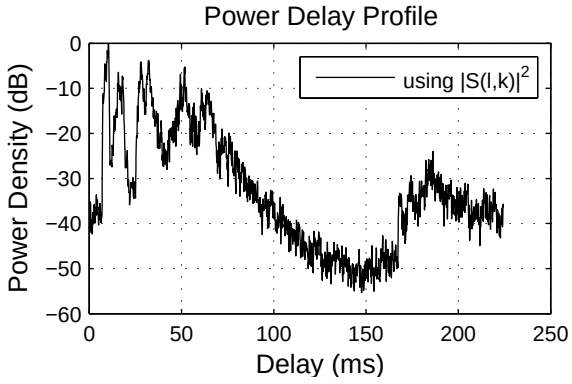

(g)

Figure 4.2: Results of using a PRBS signal of length 255: (a)Temporal Impulse response,(b)Spreading function (c) Doppler power spectrum to b., (d)Scattering function , (e)Doppler power spectrum to d. (f) Power delay profile to b.(g)Power delay profile to d.

The first probe signal to be analysed on channel 4 is the PRBS signal of length 255. The results of the simulation is shown in Figure 4.2 where the temporal impulse response has been estimated and plotted for a time window that runs over 224 ms. The impulse response shows an arrival pattern that starts with the strongest arrival at a delay of about 10 ms followed by a multiple arrival pattern that fluctuate rapidly on the left and right of a 50 ms delay; after a time gap of nearly 50 ms of negligible arrival pattern, a weaker patter of arrivals can be seen at and in the vicinity of a 200 ms delay. To exploit the statistical model of the channel, the spreading function and the scattering function have been plotted as shown in Figure 4.2 (b) and (d). Although the mathematical expressions for these functions are very unlike, they do produce similar results for most channels as can be seen for this channel. These functions goal is to show the plot of the expected power as a function of Doppler shift and delay. It is clear from the two plots that the Doppler spread pattern is exactly what is expected if they are compared to the plot of the temporal impulse. Considering the projection of the spreading and or scattering function on the Doppler frequency shift axis, the Doppler power spectrum has been estimated and plotted in Figure 4.2 (c) and (e) for comparison. The plots of the Doppler power spectrum resulting from these two functions are quite alike, except that the one resulting from the scattering function is more stochastic and demonstrates a more oscillatory pattern in the power level just below about -95 dB and proceeding downward. The oscillation pattern as seen in the plots are not due to noise but to fluctuations in the signal amplitude and phase; this can be due to instrument jitter or disturbances caused by wind and current to the transducer. The Doppler spectrum is seen to be a spike between 0 and -25 dB , and then broadened for the rest of the plot in both cases. Next, considering the projection of the spreading and or scattering function on the delay time axis, the power delay profile has been estimated and plotted in Figure 4.2 (f) and (g) for comparison. The arrival structure is in agreement with the impulse response, where we see the first group of arrivals having higher amplitudes between a delay of 0 and 50 ms. The middle segment of the plots show a downward pattern of the arrivals exhibiting deep fading down to about -50 dB and then continuing back up to about -28 dB before making a final stop at about -40 dB. Finally, taking the Fourier transform of the delay power profile and the inverse Fourier transform of the Doppler power spectrum give an estimate of the spaced frequency and the spaced time functions. The plots of these functions are shown in Figure 4.3. Finally, Tables 4.3 and 4.4 give some estimated values of the channel parameter such as the average delay spread and the Doppler spread; it was not possible to measure the coherence time of the two functions at the same points since they do not match at every point.

Tm [ms]	σ_{T_m}[ms]	ρ_{max}[mHz]	B_d[mHz]	Maximum excess delay [ms]
53.5	66.7	111	77	55.5
52.1	47.1	19.5	103	44.4

* The second row gives the values obtained from using the spreading function and the last from the scattering function

Table 4.3: This table shows the estimated values of the delay spread, rms delay spread, maximum Doppler shift, Doppler spread and the maximum excess delay spread

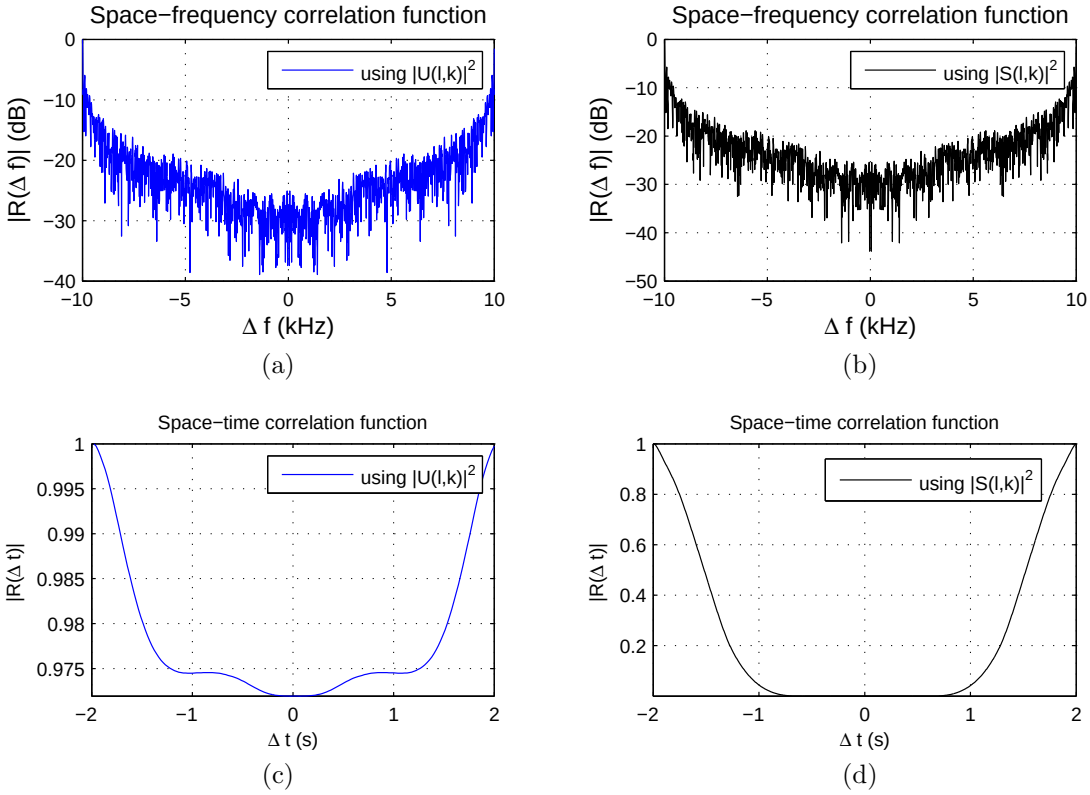

Figure 4.3: The spaced frequency and spaced time functions: (a)Spaced frequency function using the spreading function(b)Spaced frequency function using the scattering function (c) Spaced time function using the spreading function (d) Spaced time function using the scattering function

B_{c-10dB}[Hz]	B_{c-15dB}[Hz]	B_{c-20dB}[Hz]	$T_{c.975;.1}$ [s]	$T_{c.98;.25}$ [s]	$T_{c.99;.5}$ [s]
19.5	19.7	15.7	2.44	2.98	3.42
19.4	17.7	18.8	2.29	2.65	3.02

* The second row gives the values obtained from using the spreading function and the last from the scattering function

Table 4.4: This table shows the estimated values of the coherence bandwidth measured at -15, -20 and -25 dB and the coherence time measured at 0.975, 0.98 and 0.99 in the second row and 0.1. 0.25 and 0.5 in the last row respectively

Simulation results for a PRBS signal of length 511

An increment in the length of the PRBS signal gives the following plots shown in Figure 4.4. If the plots are now compared to that of Figure 4.2, starting with the temporal impulse response, we observe that the strongest arrivals are no longer at the beginning; the main arrivals are now concentrated around 100 ms of which the maximum is found to be located at about 70 ms. The plot of the impulse response here can be said to be a shifted version of Figure 4.2 (a); except for the negligible arrival patterns left of the peak arrival. The plots of the corresponding spreading and scattering functions in Figure 4.4 (b) and (d) show similar effects as expected. Taking a closer look at the Doppler power

spectral in Figure 4.4 and (c) and (e), we see a decrease in the width of the pulse between -50 dB and -100 dB as compared to the previous plots shown in the corresponding plots of Figure 4.2. However, the Doppler power spectra are no longer seen to be a spike between 0 and -25 dB; they have gained some width and in addition some side lobes as well. The power delay profiles shown in Figure 4.4 (f) and (g) now show a longer length of fading at the beginning before featuring about three main arrivals and then imitating the fading pattering as described for those in Figure 4.2. Next, the plots of the channel spaced time and spaced frequency correlation have been plotted in Figure 4.5; we see some changes in these plots if we compare them to their counterparts in Figure 4.3. For instance, the bottom of the spaced time correlation function is now smoother than before. These functions were used to get an approximate estimates of the coherence time and bandwidth of the channel. A summary of the estimates of the channel important parameters are shown in Tables 4.5 and 4.6

Tm [ms]	σ_{T_m}[ms]	ρ_{max}[mHz]	B_d[mHz]	Maximum excess delay [ms]
98.4	70.1	147	95.6	56.4
95.9	49.7	19.5	124	56.8

* The second row gives the values obtained from using the spreading function and the last from the scattering function

Table 4.5: This table shows the estimated values of the delay spread, rms delay spread, maximum Doppler shift, Doppler spread and the maximum excess delay spread

B_{c-6dB}[Hz]	B_{c-10dB}[Hz]	B_{c-15dB}[Hz]	$T_{c.92;.1}$ [s]	$T_{c.95;.25}$ [s]	$T_{c.98;.5}$ [s]
19.5	18.6	15.1	0.71	2.47	3.18
19.1	18.2	15.2	2.75	3.04	3.34

* The second row gives the values obtained from using the spreading function and the last from the scattering function

Table 4.6: This table shows the estimated values of the coherence bandwidth measured at -15, -20 and -25 dB and the coherence time measured at 0.92, 0.95 and 0.98 in the second row and 0.1. 0.25 and 0.5 in the last row respectively

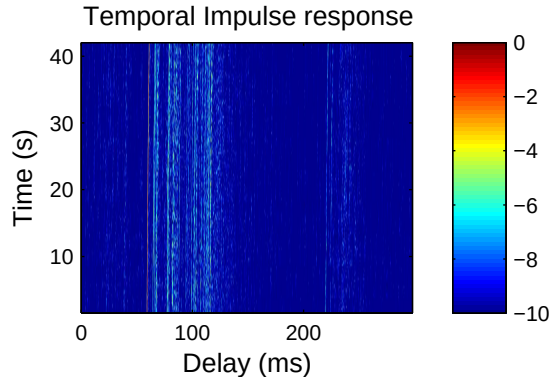

(a)

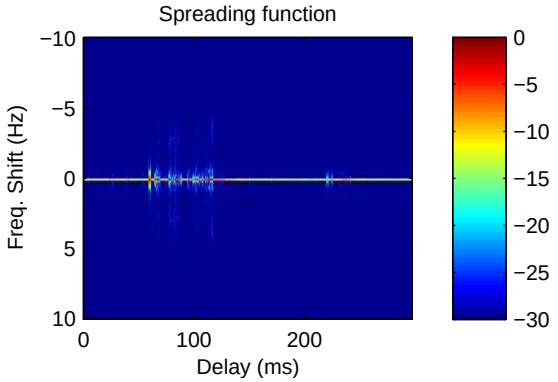

(b)

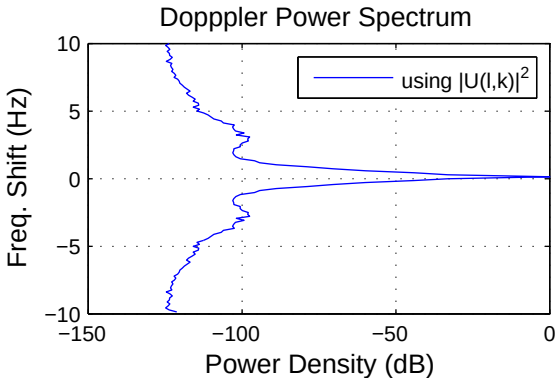

(c)

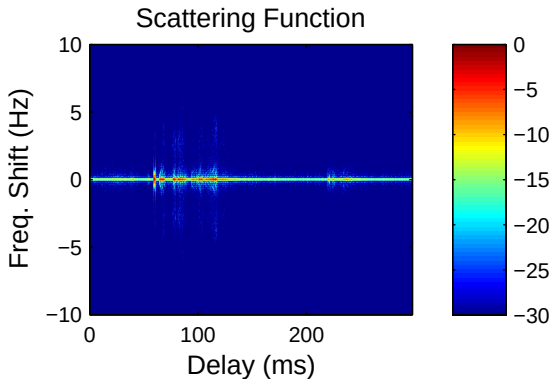

(d)

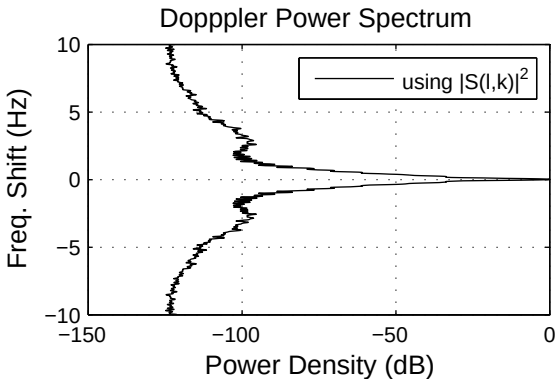

(e)

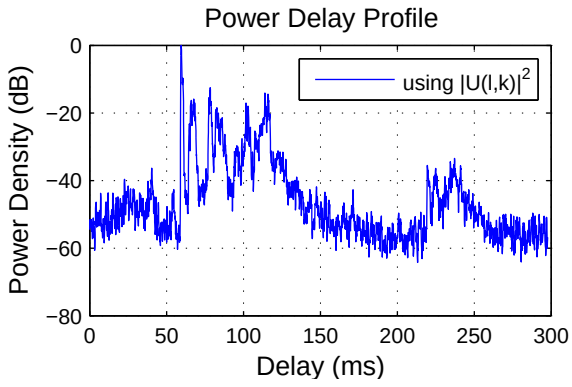

(f)

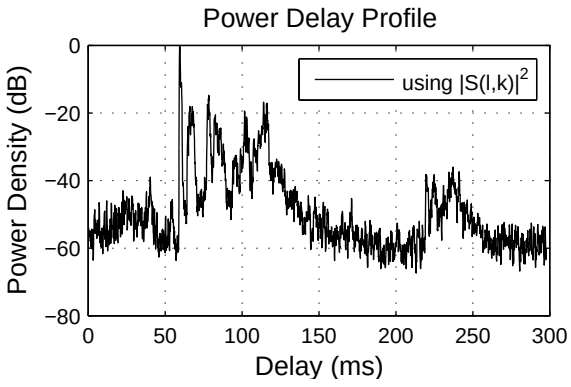

(g)

Figure 4.4: Results of using a PRBS signal of length 511: (a)Temporal Impulse response,(b)Spreading function (c) Doppler power spectrum to b., (d)Scattering function , (e)Doppler power spectrum to d. (f) Power delay profile to b.(g)Power delay profile to d.

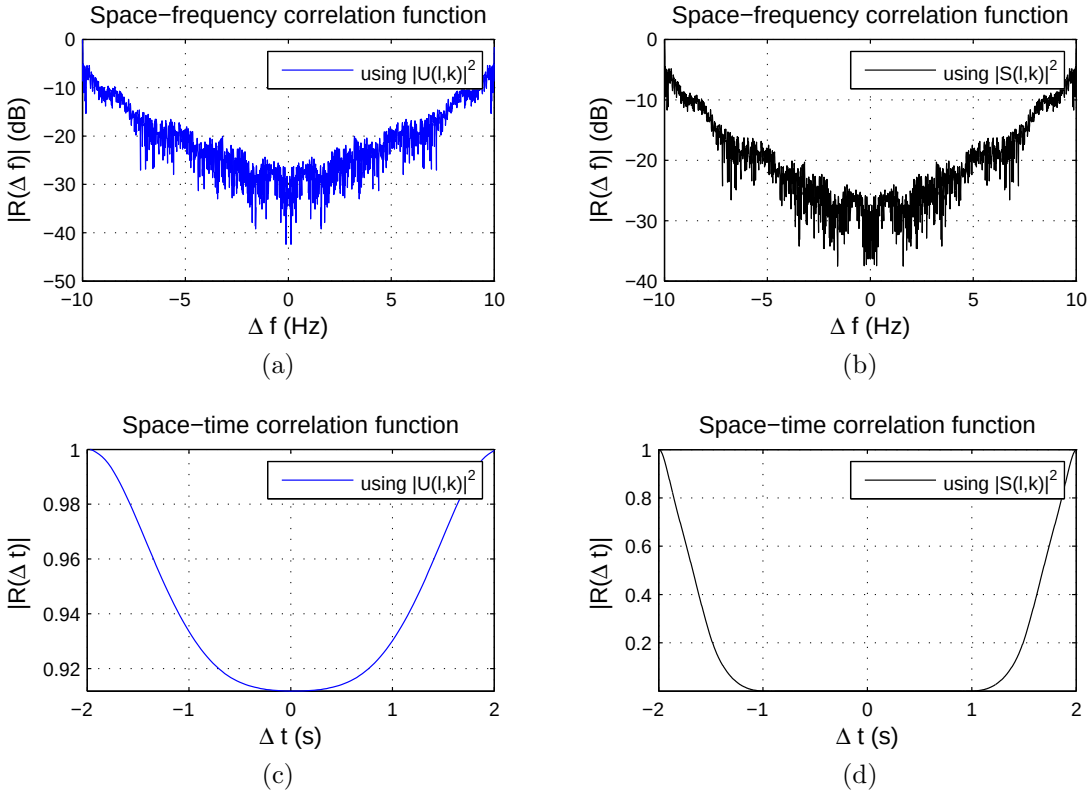

Figure 4.5: The spaced frequency and spaced time functions: (a)Spaced frequency function using the spreading function(b)Spaced frequency function using the scattering function (c) Spaced time function using the spreading function (d) Spaced time function using the scattering function

Simulation results for a PRBS signal of length 1023

The final of the PRBS signals to be analysed is the one of length 1023 corresponding to an m-sequence generated by a shift register of 10 stages in the register circuit. Proceeding with our analysis as before, we see that the high level of fluctuation in the amount of correlation is also present in Figure 4.6 (a) as in the case of the previous two cases and that the arrivals have undergone deep fading with the strongest correlation component occurring at about 17 ms. The arrival pattern in this scenario is more stable in time and amplitude. After an empty gap of nearly 100 ms (between 100 ms to 200 ms), one strong arrival can be seen at about 178 ms followed by a couple of faded arrivals; we can also see some contribution to the arrival pattern from an unknown object in the vicinity of a 300 ms delay. The corresponding spreading and scattering functions shown in Figure 4.6 (b) and (d) show minimum spread in Doppler shifts than their counterparts in Figures 4.2 and 4.4. The plots in Figure 4.6 (c) and (e) of the Doppler power spectra reveal a further gain in the spectral width below about -20 dB, and a further increased in side lobes having peak value at about -98 dB then those introduced in Figure 4.4. Next, comparing the plots of the power delay profile in Figure 4.6 (f) and (g) to those in Figure 4.2 (f) and (g), it can be concluded that the plots obtained here are just a longer version extending up to about 444 ms.

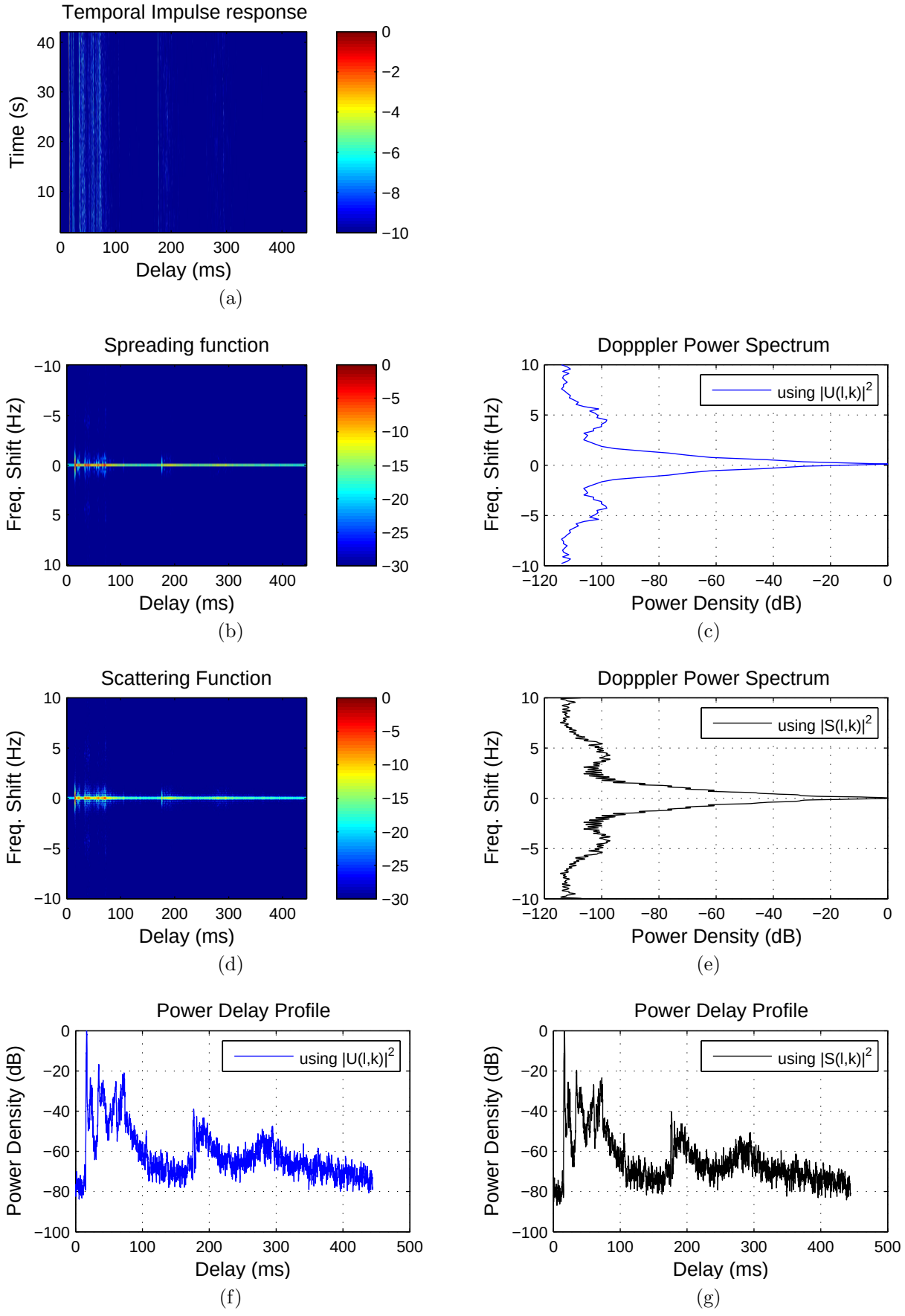

Figure 4.6: Results of using a PRBS signal of length 511: (a)Temporal Impulse response,(b)Spreading function (c) Doppler power spectrum to b., (d)Scattering function , (e)Doppler power spectrum to d. (f) Power delay profile to b.(g)Power delay profile to d.

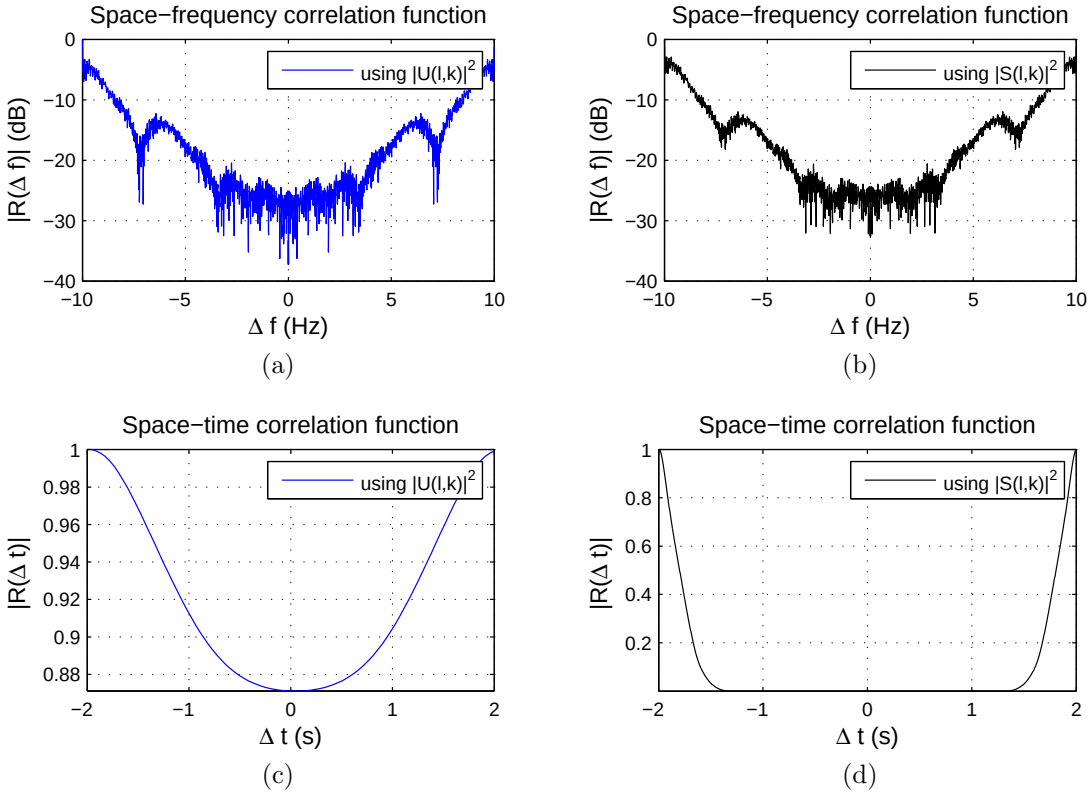

Figure 4.7: The spaced frequency and spaced time functions: (a)Spaced frequency function using the spreading function(b)Spaced frequency function using the scattering function (c) Spaced time function using the spreading function (d) Spaced time function using the scattering function

The result of plotting the spaced frequency and spaced time correlation functions is shown next in Figure 4.9. The shape of the spaced frequency correlation function has changed a lot as compared to those in Figures 4.3 and 4.5. On the other hand, comparing the two plots of the spaced time correlation functions obtained from using the spreading and scattering functions, we see that the one obtained from the spreading function seems to be approaching the other as the length of the input signal increases. A summary of the estimates of the channel important parameters are shown in Tables 4.7 and 4.8

Tm [ms]	σ_{T_m}[ms]	ρ_{max}[mHz]	B_d[mHz]	Maximum excess delay [ms]
60.4	102.5	109.9	130.7	56
56.2	71.9	19.5	169.8	56

* The second row gives the values obtained from using the spreading function and the last from the scattering function

Table 4.7: This table shows the estimated values of the delay spread, rms delay spread, maximum Doppler shift, Doppler spread and the maximum excess delay spread

B_{c-3dB}[Hz]	B_{c-6dB}[Hz]	B_{c-10dB}[Hz]	$T_{c.88;.1}$ [s]	$T_{c.92;.25}$ [s]	$T_{c.96;.5}$ [s]
19.33	18.6	18.4	1.01	2.15	2.86
19.77	18.1	16.43	3.2	3.38	3.60

* The second row gives the values obtained from using the spreading function and the last from the scattering function

Table 4.8: This table shows the estimated values of the coherence bandwidth measured at -15, -20 and -25 dB and the coherence time measured at 0.88, 0.92 and 0.96 in the second row and 0.1. 0.25 and 0.5 in the last row respectively

Simulation results for an LFM signal

Our final signal to be analysed is the linear frequency modulation(LFM) signal. The results of exciting channel 4 with an LFM signal is shown in Figure 4.8. Comparing the temporal impulse responses obtained from exciting the channel with a PRBS signal of different lengths to the one shown here in Figure 4.8 (a), we see an arrival pattern that is more stable in both time and amplitude and concentrated in one area; even though later arrivals show some degree of fading as in the other three cases. The strongest arrival is seen to appear at about 12 ms. The corresponding spreading and scattering functions to this channel show the minimum spread in Doppler shift of the four cases studied. Taking a look at the Doppler power spectra in Figures (c) and (e), we see a significant increase in the main sidelobes and a broader spectra. Next, Figure 4.8 (f) and (g) show a significant change in the arrival pattern of the power delay profiles. Only one main arrival and a couple of weaker arrivals with insignificant amplitudes can be identified; the rest have interacted with the sea floor multiple of times and can be considered as noise floor (see appendix B?). Finally, as in the case of the PRBS signals, Figure 4.8 show plots of the spaced frequency and spaced time correlation functions; the frequency correlation function can be identified as a noise-like notched filter. A summary of the estimates of the channel important parameters are shown in Tables 4.9 and 4.10.

Tm [ms]	σ_{T_m}[ms]	ρ_{max}[mHz]	B_d[mHz]	Maximum excess delay [ms]
18.5	19.4	200	45.2	18.9
17.9	15	19.5	81.3	18.9

* The second row gives the values obtained from using the spreading function and the last from the scattering function

Table 4.9: This table shows the estimated values of the delay spread, rms delay spread, maximum Doppler shift, Doppler spread and the maximum excess delay spread

B_{c-3dB}[Hz]	B_{c-6dB}[Hz]	B_{c-10dB}[Hz]	$T_{c.97;.1}$ [s]	$T_{c.98;.25}$ [s]	$T_{c.99;.5}$ [s]
13.62	9.82	6.46	1.28	2	2.66
13.38	9.24	6.22	3.14	3.32	3.52

* The second row gives the values obtained from using the spreading function and the last from the scattering function

Table 4.10: This table shows the estimated values of the coherence bandwidth measured at -15, -20 and -25 dB and the coherence time measured at 0.97, 0.98 and 0.99 in the second row and 0.1. 0.25 and 0.5 in the last row respectively

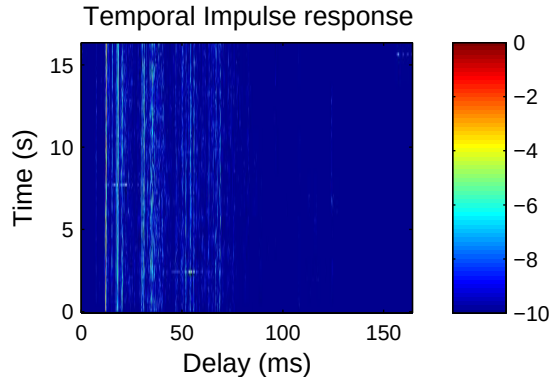

(a)

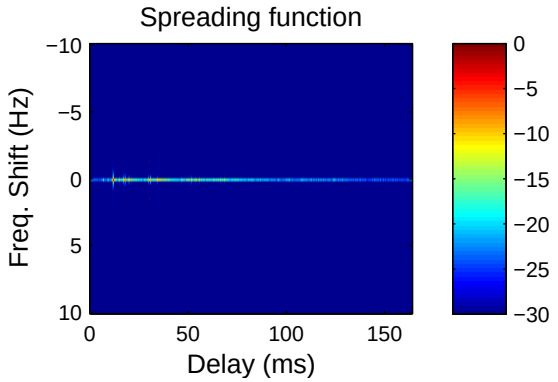

(b)

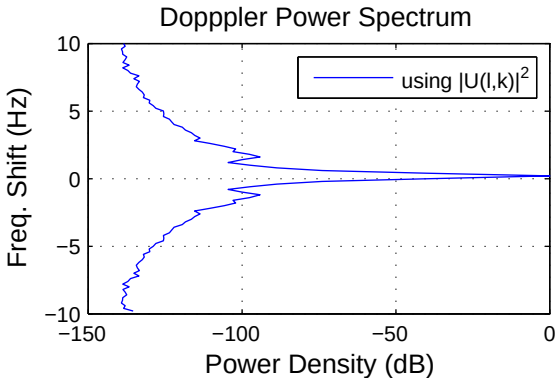

(c)

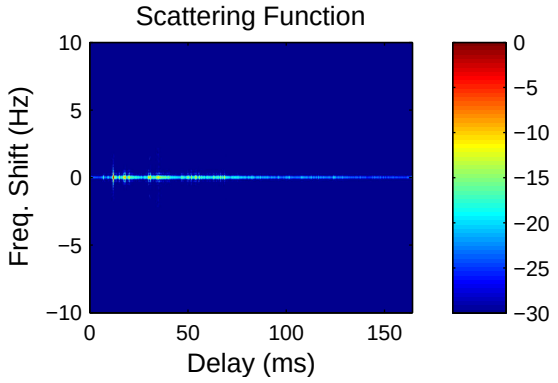

(d)

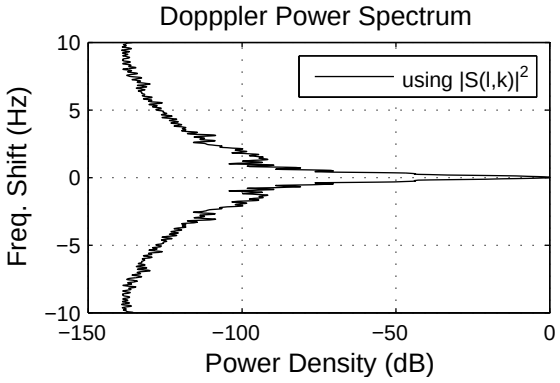

(e)

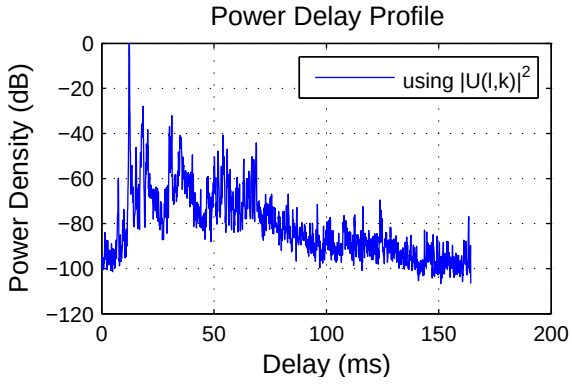

(f)

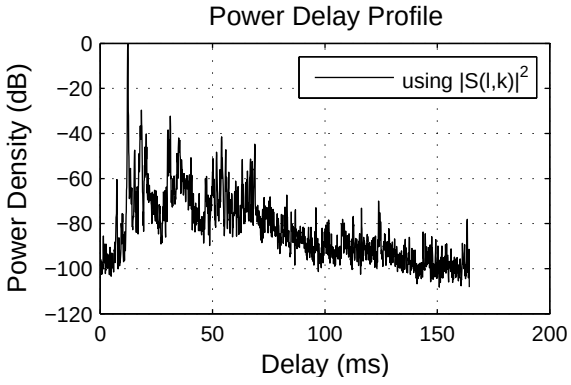

(g)

Figure 4.8: Results of using an LFM signal: (a)Temporal Impulse response,(b)Spreading function (c) Doppler power spectrum to b., (d)Scattering function , (e)Doppler power spectrum to d. (f) Power delay profile to b.(g)Power delay profile to d.

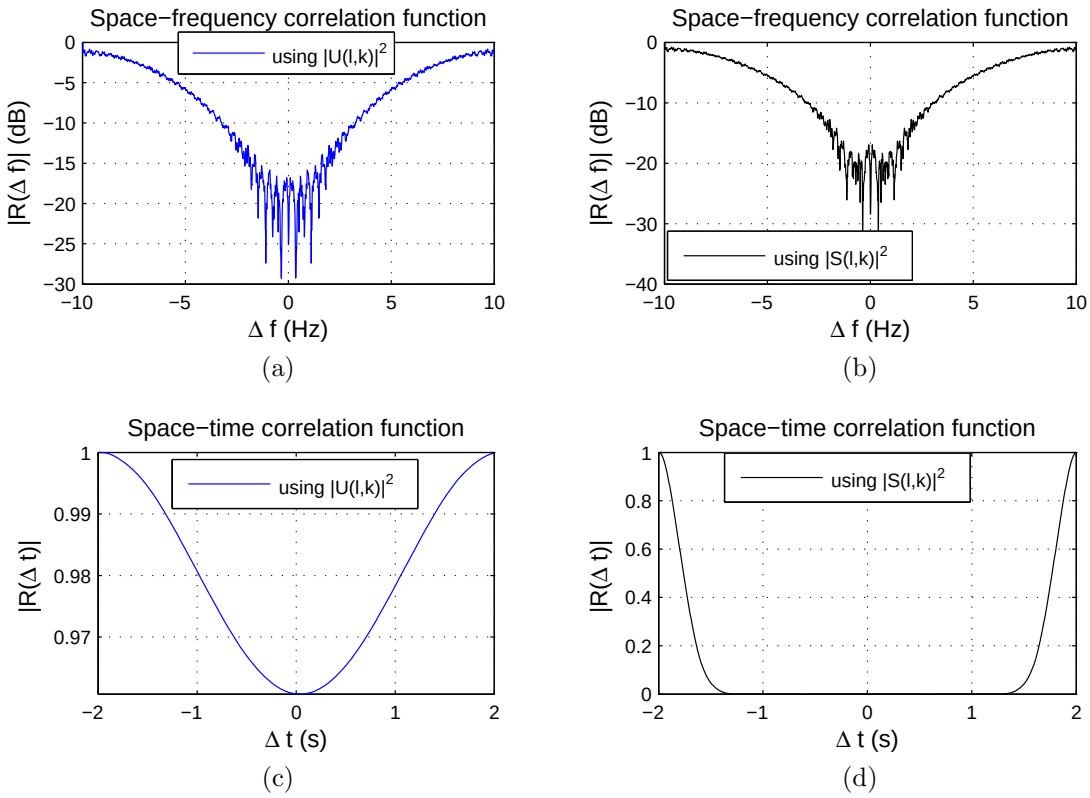

Figure 4.9: The spaced frequency and spaced time functions: (a)Spaced frequency function using the spreading function(b)Spaced frequency function using the scattering function (c) Spaced time function using the spreading function (d) Spaced time function using the scattering function

Summary of the Results

Our analysis of channel 4 with the PRBS signal has shown that as the length of the signal increases, the width of the Doppler power spectrum increases and a further increased is observed in sidelobes which can be undesirable depending on their amplitude level. Fewer arrivals are estimated with the majority having very little amplitudes as the result of deep fading. Please see appendix B for a clearer picture of these observations. Application of the LFM signal to the channel reveal similar effects; the Doppler power spectrum gained its most width and only a single peak arrival is clearly seen in the plot of the power delay profile. At this point, the choice of the transmitted signal waveform is not straight forward. Depending on the application of the communication system and how much Doppler shift is to be tolerated by the receiver, according to [1] the choice between a PRBS and an LFM waveforms is an issue that lies in the compromise of Doppler tolerance. For the sake of properly estimating the scattering function, the PRBS signal is more suitable because of its narrow ambiguity function in both delay and Doppler and in this analysis, the signal of length 255 may be preferred over the rest.

Chapter 5

Summary

An underwater acoustic communication channel has been characterized based on experimental data. The method of characterizing the channel was based on estimation of the channel temporal impulse response by emitting probe signals with well behave autocorrelation functions, and using the result to get an estimate of the channel spreading and scattering functions; from these functions, the channel correlation functions such as the delay power profile, the Doppler power spectrum, and the spaced time and frequency functions were estimated and presented in the form of figures. The estimated values of the average delay spread, rms delay spread, Doppler shift, Doppler spread, coherence time, coherence bandwidth and maximum excess delay of the power delay profile are presented in the form of tables. The channel characterized in this report was found to fluctuate in amplitude and suffered from fading; some degree of Doppler shifts were observed in the channel and were mainly caused by the boat carrying the transmitter. Although there were a total of 20 channels measured during the Trondheim Fjord experiments, but it was not necessary to analyze all of them in this master thesis. The goal of the project was to be able to characterize an underwater communication channel based on experimental data with the aid of matlab. The results presented in this report were found to be consistent with theory and can be compared with the work found in [3], [4] and [2]. Since the procedure for characterizing the channel in this report is quite similar to the remaining channels, a future work will be to apply the procedure to the balance 19 channels.

[18]

Bibliography

[1] T. Eggen, A. Baggeroer, and J. Preisig, "Communication over doppler spread channels. part i: Channel and receiver presentation," *IEEE Journal of Oceanic Engineering*, vol. 25, no. 1, pp. 62–71, 2000.

[2] B. Borowski, "Characterization of a very shallow water acoustic communication channel," in *OCEANS 2009, MTS/IEEE Biloxi-Marine Technology for Our Future: Global and Local Challenges*, p. 110, 2009.

[3] P. van Walree, "Channel sounding for acoustic communications: techniques and shallow-water examples," *Norwegian Defence Research Establishment (FFI), Tech. Rep. FFI-rapport*, vol. 7, 2011.

[4] P. A. van Walree and G. Bertolotto, "Characterization of an acoustic communication channel with pseudorandom binary sequences," *Proceedings of Underwater Acoustic Measurements UAM2007, Heraklion, Crete*.

[5] P. M. Shankar, *Introduction to wireless systems*. New York: J. Wiley, 2002.

[6] A. Goldsmith, *Wireless communications*. Cambridge; New York: Cambridge University Press, 2005.

[7] J. G. Proakis and M. Salehi, *Digital communications*. Boston: McGraw-Hill, 2008.

[8] J. G. Proakis and M. Salehi, *Communication systems engineering*. Upper Saddle River, N.J.: Prentice Hall, 2002.

[9] R. Diamant and L. Chorev, "Emulation system for underwater acoustic channel," in *International Undersea Defence Technology Europe conference (UDT)*, 2005.

[10] X. Lurton, *An introduction to underwater acoustics: principles and applications*. Heidelberg; New York; Oxford: Springer Verlag, published in association with Praxis Publishing, 2010.

[11] P. Bello, "Characterization of randomly time-variant linear channels," *Communications Systems, IEEE transactions on*, vol. 11, no. 4, p. 360393, 1963.

[12] "RMS delay spread measurement (theory) : Wireless lab : Electronics & communications : IIT DELHI virtual lab."

[13] M. I. Skolnik, *Introduction to radar systems*. Boston: McGraw Hill, 2001.

[14] B. R. Mahafza, *Radar systems analysis and design using Matlab*. Boca Raton: Chapman & Hall/CRC, 2000.

[15] B. S. Sharif, J. Neasham, O. R. Hinton, and A. E. Adams, "A computationally efficient doppler compensation system for underwater acoustic communications," *Oceanic Engineering, IEEE Journal of*, vol. 25, no. 1, p. 5261, 2000.

[16] A. Quinquis, *Digital signal processing using MATLAB*. London; Hoboken, NJ: ISTE ; Wiley, 2008.

[17] "7117992 communication systems simon haykin 4ed."

[18] M. Smedsrud, "Acharacterization of underwater acoustic communication channels by computer simulations," Master's thesis, Norwegian University of Science and Technology, June 2005.

.1 Appendix A : Matlab Program Codes

C1

The purpose of this block of matlab code is to process the data and perform an estimation of the channel impulse response when it is excited by either an LFM signal of a PRBS signal; this particular example is done for an m-sequence of length 1023.

```
function ReadData_PnBPSK10_ScatteringEstimate()

% Load input signal

lfmpath = '..\TRANSMIT_SIGNALS\M_SEQ\...
SQUARE-ROOT_RAISED_COSINE\M10\fc10000Hz\BPSK\Fw-over-fc_0.35\';
lfmnam = 'Tfilter_BPSK_fc10000Hz_Bw-fc-ratio0.35.mat';
disp([lfmpath lfmnam])
load([lfmpath lfmnam],'x','tx','fc','Bw','Fs')

% Duration of LFM signal (2746 samples at 192 kHz smp freq)
Tlfm = length(x)/192000;
% Duration of gap between 2 succesive LFM
Tgap = 0.150;

%%%%%%%%%%%%%%%%%%%%%%%%%%%%%%%%%%%%%%%%%%%%%%%%%%%%%%%%%%%%%%%%%%%%%%%%%%%%
% The signal can be processed by making use of the passband signal x ...
    %
% as it is, however, the baseband procedure is preferred. Comment ...
   the %
% baseband method if you wish to work with the passband signal. ...
         %
%%%%%%%%%%%%%%%%%%%%%%%%%%%%%%%%%%%%%%%%%%%%%%%%%%%%%%%%%%%%%%%%%%%%%%%%%%%%


% Baseband formulation of the passband signal x

xb = hilbert(x).*exp(-1i*2*pi*fc.*tx);
% figure
% subplot(121);
% plot(tx,real(xb));grid; %hold on;
% title('Equivalent baseband signal sampled at fs = 192000, xb');

Fs_decim = 10000; % reducing the sampling frequency fs by resampling
xb = resample(xb,Fs_decim,Fs);
 tt = 0:1/Fs_decim:(length(xb)-1)/Fs_decim;
% figure
% plot(tt,real(xb),'r');grid;
% title('Equivalent baseband signal resampled at fs = 5000, xb');
% pause
smf = conj(flipud(xb(:)));  % matched filter to xb
Lsm = length(smf);
% figure
% plot(abs(conv(xb,smf.')));
% title('Pulse compression of xb with its matched filter at fs = 5000');
% pause
%

% Decimation factor
```

```
47 % Fs_decim = 10000;
48
49 % Passband formulation of the passband signal x
50 %
51 % % figure
52 % % plot(tx,x); grid; hold on;
53 % % title('Passband signal sampled at fs = 192000');
54 %
55 % x = resample(x,Fs_decim,Fs);  % resampled transmitted signal
56 % Lx= length(x);
57 % % tt = 0:1/Fs_decim:(Lx-1)/Fs_decim;
58 % % plot(tt,x,'r');
59 %
60 % smf = conj(flipud(x(:)));
61 % Lsm = length(smf);
62 % % pause
63 % %  figure
64 % %  plot((0:1/Fs_decim:(2*length(s)-2)/Fs_decim),abs(conv(s,smf)))
65 % %
66
67
68 datapath ='../DATA/';     % Set the data path for processing
69
70 % Fs_r = 100000;          % Sampling rate of receive signal
71 % Input LFM duration : 2746 samples at 192 kHz sampling rate
72 % Loop over 16 channels
73
74
75 % Processing the data to get the received signal y.
76 for iper = 1 %1:5
77
78     disp('Period'); disp(iper);
79
80     for ich = 4 %1:20
81        disp('Channel'); disp(ich);
82        y = [];         % initialize received signal vector (or matrix)
83
84         readpath = ['./P' num2str(iper) '/']; % Path to the forder ...
               containing
85                                                % the measured ...
                                                     channels : P1
86
87         readfile = ['D1ST3_CH' num2str(ich) '_P' num2str(iper) '.dat'];
88         % Vector containg the channels; channel 4 in this case
89
90         fid = fopen([datapath readpath readfile],'r'); % Open data file;
91               % that is, open the file called DATA, then P1 and then the
92               % channel(s) for reading only.
93
94         y = fread(fid,inf,'float64'); % Fill the received signal vector
95                                       % with the data (channel 1 through
96                                       % 20); only channel 4 in this case
97         fclose(fid); % close file
98         load([datapath readpath 'RecSamplingRate.mat'],'Fs_r');% ...
               Load the
99                                                    % Sampling ...
                                                        Frequency Fs_r
100
```

```
101         figure, subplot(2,1,1)
102         plot(y)
103         title('The  received signal y');
104         pause(2)
105
106         y = squeeze(y(1.058e7:1.498e7)).'; % Extracting portion of ...
                the re-
107                                            % ceived signal to be ...
                                                  processed.
108         Ly = length(y);
109         ty = 0:1/Fs_r:(Ly-1)/Fs_r; subplot(2,1,2)
110         plot(ty,y)
111
112
113 %         y = resample(y,Fs_decim,Fs_r);
114 %         Ly = length(y);
115 %         ty = 0:1/Fs_decim:(Ly-1)/Fs_decim;
116 %
117 %         figure,
118 %         plot(ty,y);title('A truncated version of the received ...
        signal y');
119 %         pause
120
121         % Passeband formulation of the passband received signal y
122
123 %         Lc = Ly + Lsm - 1;                  % length of convolution
124 %         tc = 0:1/Fs_decim:(Lc-1)/Fs_decim; % time vector
125 %         y_pc = abs(conv(y,smf.'));
126 %
127 %         figure
128 %         plot(tc,y_pc)
129 %         title('Pulse Compressed signal')
130 %         xlabel('time [sec]')
131
132
133         % Baseband formulation of the passband received signal y
134
135         yb = hilbert(y).*exp(-1i*2*pi*fc.*ty); % BaseBand equivalent ...
                of the
136                                                %received signal y
137         yb = resample(yb,Fs_decim,Fs_r);
138         Lyb = length(yb);
139
140         tyb = 0:1/Fs_decim:(Lyb-1)/Fs_decim;
141         figure
142         plot(tyb,real(yb));
143         title('Baseband equivalent of the truncated received signal, ...
                yb');
144         xlabel('time [sec]');
145         pause(2)
146
147         Lyb = length(yb);
148         Lc = Lyb + Lsm - 1; % convolution length
149         tyc = 0:1/Fs_decim:(Lc-1)/Fs_decim;
150         y_pc = abs(conv(yb,smf.'));
151
152         figure
153         plot(tyc,y_pc);
```

```
154         title('Pulse Compression');
155         xlabel('time [sec]') ;
156         pause(2)
157
158
159 df = -10:0.1:10; % Doppler resolution
160 Nd = length(df);
161 for id = 1:Nd
162         if ~mod(id,1), disp([num2str(id) '/' num2str(Nd)]),end
163       % Pulse compression (convolution with matched filter) - Baseband
164         Lc = Lyb + Lsm - 1; % length of convolution
165         tyc = 0:1/Fs_decim:(Lc-1)/Fs_decim; % time vector
166         y_pc(id,1:Lc) ...
              =abs(conv(yb,(smf.').*exp(-1i*2*pi*df(id).*tt)));% doppler
167        % matched filter
168
169          % Start stacking
170 %          init_smp = 1.69e4; %floor(1.75*Fs_decim);%
171 %          N_smp_lfmgap = round((Tlfm + Tgap)*Fs_decim);
172 %          for ilfm = 1
173 %              smpi = init_smp + (ilfm-1)*N_smp_lfmgap;
174 %              smpf = smpi + N_smp_lfmgap -1;
175 %              n_wind = smpi:1:smpf;
176 %              %PDP(ilfm,1:length(n_wind)) = squeeze(y_pc(n_wind));
177 %           PDP(ilfm,id,1:length(n_wind)) = squeeze(y_pc(id,n_wind));
178 %          end
179
180          %imagesc(PDP)
181          %colormap(hot)
182 end
183 % y_pc=y_pc(:,97901);
184 t_geo = []; % the running time
185   init_smp = 1.91e4; %floor(1.75*Fs_decim);%
186          N_smp_lfmgap = round((Tlfm + Tgap)*Fs_decim);
187          t_del = 0:1/Fs_decim:(N_smp_lfmgap-1)/Fs_decim;
188          for ilfm = 1:91
189              smpi = init_smp + (ilfm-1)*N_smp_lfmgap;
190              t_geo = [t_geo smpi/Fs_decim];
191              smpf = smpi + N_smp_lfmgap -1;
192              n_wind = smpi:1:smpf;
193           %   PDP(ilfm,1:length(n_wind)) = squeeze(y_pc(n_wind));
194           %ytmp = squeeze(y_pc(1:Nd,n_wind));
195 %          PDP(ilfm,1:Nd,1:length(n_wind)) = (ytmp./max(abs(ytmp)));
196          PDP(ilfm,1:Nd,1:length(n_wind)) =squeeze(y_pc(1:Nd,n_wind));
197          end
198 %            figure, imagesc(PDP); % imagesc(squeeze(PDP(ilfm,:,:)));
199  end
200 end
201 % %save('PulseCompression','s_pc_trunc','t_pc_trunc','Fs_r')
202 %
203 filename = '.\RxPNBPSK10.mat'
204         save(filename)
```

C2

The purpose of this block of matlab code is to perform estimation of the channel temporal impulse response from which the spreading and scattering functions are obtained. Fur-

thermore, the remaining correlation functions such as the power delay profile and Doppler power spectrum as well as the spaced time and spaced frequency functions and parameters such as the delay spread, Doppler spread, coherence time and coherence bandwidth of the channel are obtained. For short, all results in chapter 4 are processed from this file.

```
clc;
close all;
clear all;


%%%%%%%%%%%%%%%%%%%%%%%%%%%%%%%%%%%%%%%%%%%%%%%%%%%%%%%%%%%%%%%%%%%%%%%
% This file is meant for estimating the follwing :                      %
% Temporal impulse response, Spreading function, Scattering function %
% Power Delay Profile and Doppler Power Spectrum                        %
% To get a quick understanding of the code please use the following  %
% two references :                                                      %
% 1. Channel Sounding for Acoustic Communications: techniques        %
% and shallow-water examples [Paul van Walree] April 11, 2011        %
% 2. Characterization of an Acoustic Communication Channel with      %
% Pseudorandom Binary Sequences [P. A. van Walreea and G. Bertolottob]
%%%%%%%%%%%%%%%%%%%%%%%%%%%%%%%%%%%%%%%%%%%%%%%%%%%%%%%%%%%%%%%%%%%%%%%

%  load('RxPNBPSK8.mat');   % Data for the BPSK signals for m = 8,9,10
%  load('RxPNBPSK9.mat');
%  load('RxPNBPSK10.mat');
%  load('RxPNBPSK11.mat');
%  load('RxLFM.mat');       % Data for the LFM signal

% sy_pc = sum(y_pc,2)/Lc;
% length(sy_pc);
% [maxypc,imaxypc] = max(sy_pc);
% disp(df(imaxypc));
% h = squeeze(PDP(:,imaxypc,:));   % The channel

%    save  h8 h ilfm t_del t_geo
%    save  h9 h ilfm t_del t_geo
%    save h10 h ilfm t_del t_geo
%    save h11 h ilfm t_del t_geo
%    save LFM h ilfm t_del t_geo

%    load h8
%    load h9
%    load h10
%    load h11
   load LFM

%% (A)see figure(1) Processing the correlation equations : Use the ...
    m-file
% called PlotsandOutput to view plots and calculations
h1 = abs(h)/max(max(abs(h))); % The channel: Eq 4.1 [Paul van Walree]
h1db = 10*log10(h1);
idx= h1db<-10;    % Check if value is less than -10 dB
h1db(idx)=-10;    % set all values less than -10dB equal -10 dB

%% (B)see figure(2) Spreading function using Eq 4.2 from
```

```
hspread = fft(h, [],1);                                % Eq 4.2 from ref. [1]
hspread = fftshift(hspread,1);                         % Just to include ...
    negative
                                                       % center frequency
hspread = power(abs(hspread),2);                       % Modulus square
hnormsp = abs(hspread)/max(max(abs(hspread)));         % Normalized to maximum
% hnormsp = 10*log10(hnormsp);                             % amplitude of 1
% idx1= hnormsp<-30;
% hnormsp(idx1)=-30;


%% (C) see figure(3) Scattering function using Eq 4 from ref. [2]
NFFT = 1024;
hscatter = ifft((fft(h, NFFT).^2));
hscatter = fft(hscatter);              % The scattering function eq 4
hscatter = fftshift(hscatter,1);
hnormsc = abs(hscatter)/max(max(abs(hscatter)));
% hnormsc = 10*log10(hnormsc);
% idx= hnormsc<-30;
% hnormsc(idx)=-30;

%% (D) see figure(4)Power Delay Profile as defined in Eq 4.3
% using Eq 4.2 (the spreading function)  [1]
PDP4_2 = sum(abs(hspread).^2);
PDP4_2 = abs(PDP4_2)/max(max(PDP4_2)); % Normalize maximum value to 1
% PDP4_2= mag2db(PDP4_2); % dB equivalent

%% (E) see figure(5)Power Delay Profile as defined in Eq 4.3 [1]
% using 4(the scattering function) [2]
PDP4 = sum(abs(hscatter).^2);
PDP4 = abs(PDP4)/max(max(abs(PDP4)));
% PDP4 = mag2db(PDP4);

%% (F) see figure(6) Doppler Power Spectrum as defined in Eq 4.4 [1] and
% using the spreading function using Eq. 4.2
DPS4_2 = sum(abs(hspread').^2);
DPS4_2 = abs(DPS4_2)/max(max(abs(DPS4_2)));
% DPS4_2 = mag2db(DPS4_2);
fspread = -10:20/length(DPS4_2):10;  % frequency resolution
fspread = fspread(1,2:end);

 %% (G) see figure(7) Doppler Power Spectrum as defined in Eq 4.4 [1]
% using the scattering function Eq 4 [2]
DPS4 = sum(abs(hscatter').^2);    % Doppler power spectrum
DPS4 = abs(DPS4)/max(max(DPS4));
% DPS4 = mag2db(DPS4);
fscatter = -10:20/length(DPS4):10; % frequency resolution
fscatter = fscatter(1,2:end);

 %% (H)see figure(8)The space-frequency correlation function using ...
    the spreading function
 fspace = (-10:20/length(PDP4_2):10); % Freq resolution in Hz
 fspace = fspace(1,2:end);
 PDPspace = fft(sum(abs(hspread).^2)); % Spaced-freq. function
 PDPspace = abs(PDPspace)/max(max(abs(PDPspace)));
%  PDPspace = 10*log10(PDPspace);

%% (I)see figure(9) The space frequency correlation function using ...
```

```
    the scattering function
106  fspace4 = -10:20/length(PDP4):10; % frequency resolution in Hz
107  fspace4 = fspace4(1,2:end);
108  PDPspace4 = fft(sum(abs(hscatter).^2)); % The spaced-frequency ...
       correlation function
109  PDPspace4 = abs(PDPspace4)/max(max(abs(PDPspace4)));
110 %  PDPspace4 = 10*log10(PDPspace4);
111
112 %% (J)see figure(10)The spaced time correlation function using the ...
       spreading function 4.2
113  DPSpacetime4_2 = ifft(sum(abs(hspread').^2)); % The space time ...
       correlation function
114  DPSpacetime4_2 = abs(DPSpacetime4_2)/max(max(abs(DPSpacetime4_2)));
115 %  DPSpacetime4_2 = 10*log10(DPSpacetime4_2);
116  aT4_2 = -2:4/(length(DPS4_2)):2;
117  aT4_2 = aT4_2(1,2:end);
118
119 %% (K)see figure(11) The space time correlation function using the ...
       scattering function
120  DPSpacetime4 = ifft(sum(abs(hscatter').^2));   % The space time ...
       correlation function
121  DPSpacetime4 = abs(DPSpacetime4)/max(max(abs(DPSpacetime4)));
122 %  DPSpacetime4 = 10*log10(DPSpacetime4);
123  aT4 = -2:4/(length(DPS4)):2;
124  aT4 = aT4(1,2:end);
125
126  %% (L) Estimating the delay spread, rms delay spread, maximum
127  %  doppler shift and   Doppler spread
128
129 %(1)Finding the average and rms Delay spreads using Eq. 4.2
130 PDPave4_2 = sum(t_del.*sum(abs(hspread).^2))./sum(sum(abs(hspread).^2));
131 PDPrms4_2 = sqrt(sum((t_del-PDPave4_2).^2.*(sum(hspread).^2))...
132             /sum((sum(abs(hspread).^2))));
133
134 % (2) Finding the average and rms Delay spreads using Eq. 4
135
136 PDPave4 = sum(t_del.*sum(abs(hscatter).^2))...
137          /sum(sum(abs(hscatter).^2));
138 PDPrms4 = sqrt(sum((t_del-PDPave4).^2.*(sum(abs(hscatter).^2)))...
139           /sum(sum(abs(hscatter).^2)));
140
141 % (3)Finding the average and rms Doppler spreads (Doppler shift and ...
       spread)
142 % using Eq. 4.2
143 Dpshift4_2 = sum(fspread.*(sum(abs(hspread').^2)))...
144              ./sum((sum(abs(hspread').^2)));
145 Dspread4_2 = sqrt(sum((fspread-Dpshift4_2).^2....
146             .*(sum(abs(hspread').^2)))./sum((sum(abs(hspread').^2))));
147
148 %(4) Finding the average and rms Doppler spread (Doppler shift and ...
       spread)
149 % Eq. 4
150 Dpshift4 = sum(fscatter.*(sum(abs(hscatter').^2)))...
151              /sum((sum(abs(hscatter').^2)));
152 Dpsread4 = sqrt(sum((fscatter-Dpshift4).^2.*(sum(abs(hscatter').^2)))...
153             /sum((sum(abs(hscatter').^2))));
154 % save Bpsk8
155 % save Bpsk9
```

```
% save Bpsk10
% save LFMsig
```

C3

This bock of code is for plotting and performing computations of the channel's parameters.

```
clear all;
close all;
% load Bpsk8
% load Bpsk9
% load Bpsk10
load LFMsig
%% (A) The temporal impulse response
figure(1);
imagesc(1e3*t_del, t_geo, h1db);
axis xy;
xlabel('Delay (ms)');
ylabel('Time (s)');
title('Temporal Impulse response');
colorbar;

%% (B) The spreading function
figure(2);
imagesc(1e3*t_del,[-5 5],hnormsp);
xlabel('Delay (ms)');
ylabel('Freq. Shift (Hz)');
title('Spreading function');
colorbar;

figure(12)
[xsp ysp]  = meshgrid(t_del,fspread);
mesh(1e3*xsp,ysp,hnormsp);
xlabel('Delay (ms)');
ylabel('Freq. Shift (Hz)');
title('Spreading Function');



%% (C) The scattering function
figure(3);
imagesc(1e3*t_del,fscatter,hnormsc);
axis xy;
xlabel('Delay (ms)');
ylabel('Freq. Shift (Hz)');
title('Scattering Function');
colorbar;
figure(13)
[xsc ysc]  = meshgrid(t_del,fscatter);
mesh(1e3*xsc,ysc,hnormsc);
xlabel('Delay (ms)');
ylabel('Freq. Shift (Hz)');
title('Scattering Function');

%% (D) The power delay profile of the spreading function Eq 4.2
```

```
figure(4)
plot(1e3*t_del,PDP4_2);grid;
xlabel('Delay (ms)');
ylabel('Power Density (dB)');
title('Power Delay Profile');
% legend('using |U(l,k)|^2')
%% (E)The power delay profile of the scattering function Eq 4
figure(5)
plot(1e3*t_del,PDP4,'k');grid;
xlabel('Delay (ms)');
ylabel('Power Density (dB)');
title('Power Delay Profile');
% legend('using |S(l,k)|^2');

%% (F) The Doppler power spectrum of the spreading function Eq 4.2
figure(6)
plot(fspread,DPS4_2);grid;
xlabel('Power Density (dB)');
ylabel('Freq. Shift (Hz)');
title('Dopppler Power Spectrum ');
% legend('using |U(l,k)|^2')

%%(G) The Doppler power spectrum of the spreading function Eq 4
figure(7)
plot(fscatter,DPS4,'k');grid;
xlabel('Power Density (dB)');
ylabel('Freq. Shift (Hz)');
title('Dopppler Power Spectrum ');
% legend('using |S(l,k)|^2')

%% (H) The spaced frequency correlation function  using the  ...
   spreading function
 figure(8)
 plot(fspace,PDPspace);grid;
 xlabel('\Delta f (Hz)');
 ylabel('|R(\Delta f)| (dB)');
 title('Space-frequency correlation function');
%  legend('using |U(l,k)|^2')

%% (I) The spaced frequency correlation function  using the ...
   scattering function
 figure(9)
 plot(fspace4,PDPspace4,'k');grid;
 xlabel('\Delta f (Hz)');
 ylabel('|R(\Delta f)| (dB)');
 title('Space-frequency correlation function');
 legend('using |S(l,k)|^2')
 set(gcf, 'color', [0 1 0])
%% (J) The space time correlation function using the spreading function
 figure(10)
 plot(ΔT4_2,DPSpacetime4_2);grid;
 xlabel('\Delta t (s)');
 ylabel('|R(\Delta t)| ');
 ylim([min( DPSpacetime4_2) max( DPSpacetime4_2)]);
 title('Space-time correlation function');
 legend('using |U(l,k)|^2')
 set(gcf, 'color', [1 0 1])
 %(K) The space time correlation function using the scattering function
```

```
figure(11)
plot(ΔT4,DPSpacetime4,'k');grid;
xlabel('\Delta t (s)');
ylabel('|R(\Delta t)| ');
ylim([min( DPSpacetime4) max( DPSpacetime4)]);
title('Space-time correlation function');
legend('using |S(l,k)|^2')
set(gcf, 'color', [1 0 1])


%% (L) Values of the estimated delay spread, rms delay spread, ...
    maximum doppler
% Doppler shifi and doppler spread

% (1) Average delay spread and rms delay spread using Eq. 4.2
  Tm4_2 = PDPave4_2
  sigma4_2 =PDPrms4_2
% (2) Average delay spread and rms delay spread using Eq. 4
  Tm4= PDPave4
  sigma4 =PDPrms4

  %(3) Average delay spread and rms delay spread in Hz using Eq 4
   fd4_2 = Dpshift4_2
    Bd4_2 = Dspread4_2

  %(4) Average delay spread and rms delay spread in Hz using Eq 4
  fd4 = Dpshift4
   Bd4 = Dpsread4
```

.2 Appendix B : Matlab Reference Plots

This appendix includes the following plots in absolute values: The spreading and scattering functions in 3-D, their corresponding Doppler power spectra and power delay profiles and the Fourier transform of the power delay profiles; in other words the spaced frequency correlation functions. Since the decibel representations of these plots exaggerate their values, an absolute value plot of them will be helpful in case of doubt.

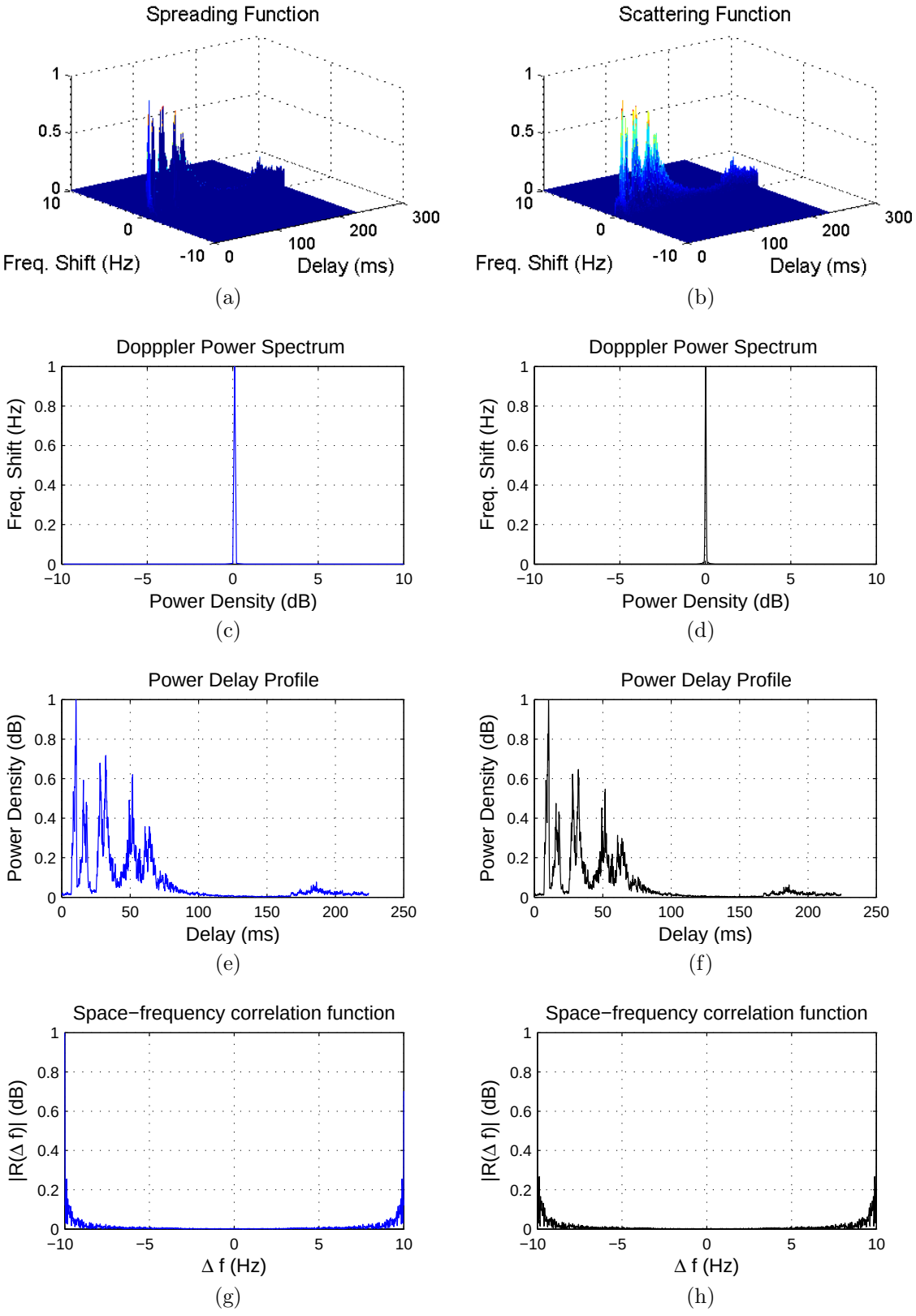

Figure 1: PRBS signal of length 255: (a)3-D spreading function(b)3-D scattering function (c) Doppler power spectrum of a. (d) Doppler power spectrum of b.(e)Power delay profile of a. (f)Power delay profile of b. (g)Spaced frequency correlation function of e. (h)Spaced frequency correlation function of f.

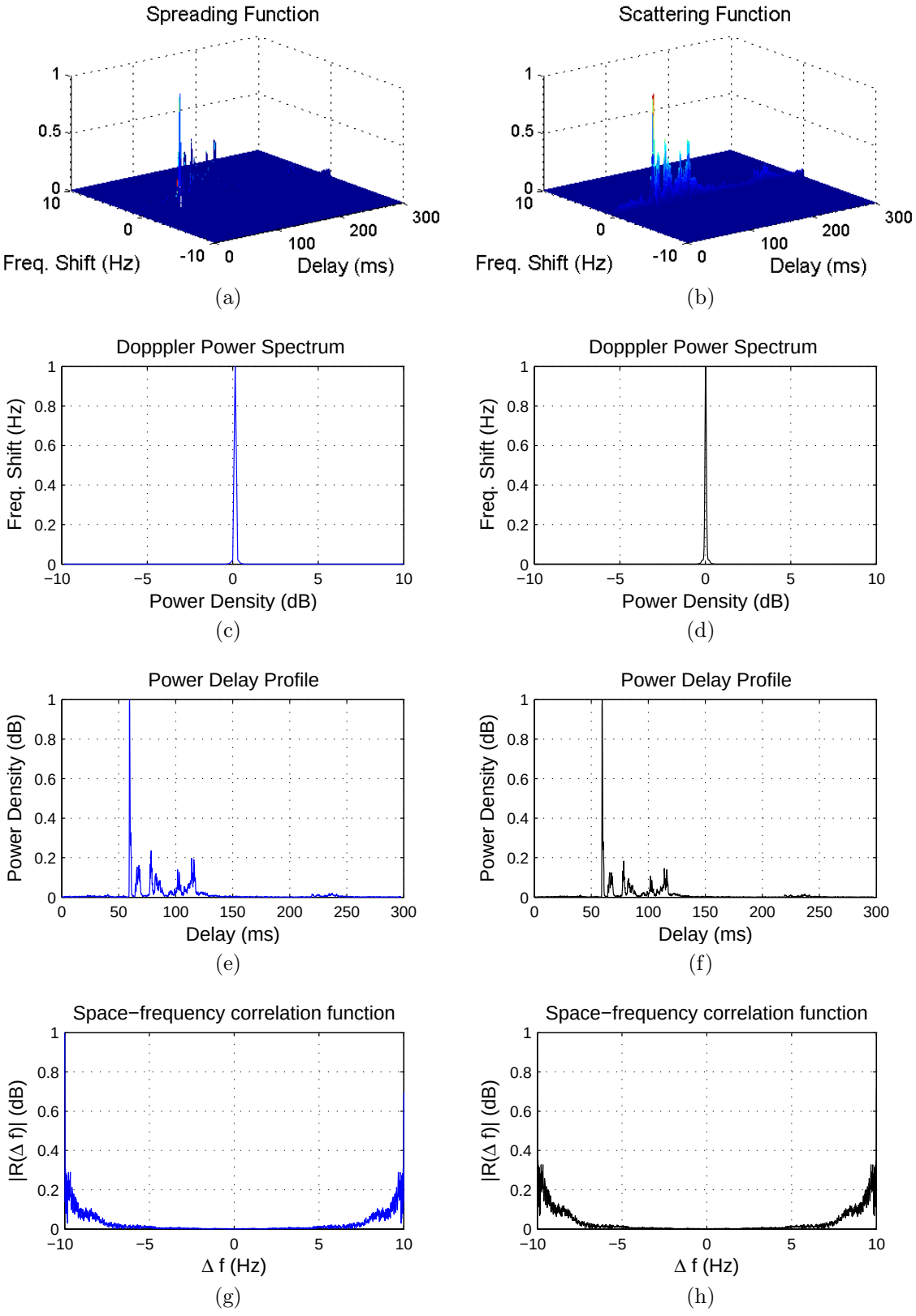

Figure 2: PRBS signal of length 511: (a)3-D spreading function(b)3-D scattering function (c) Doppler power spectrum of a. (d) Doppler power spectrum of b.(e)Power delay profile of a. (f)Power delay profile of b. (g)Spaced frequency correlation function of e. (h)Spaced frequency correlation function of f.

M10

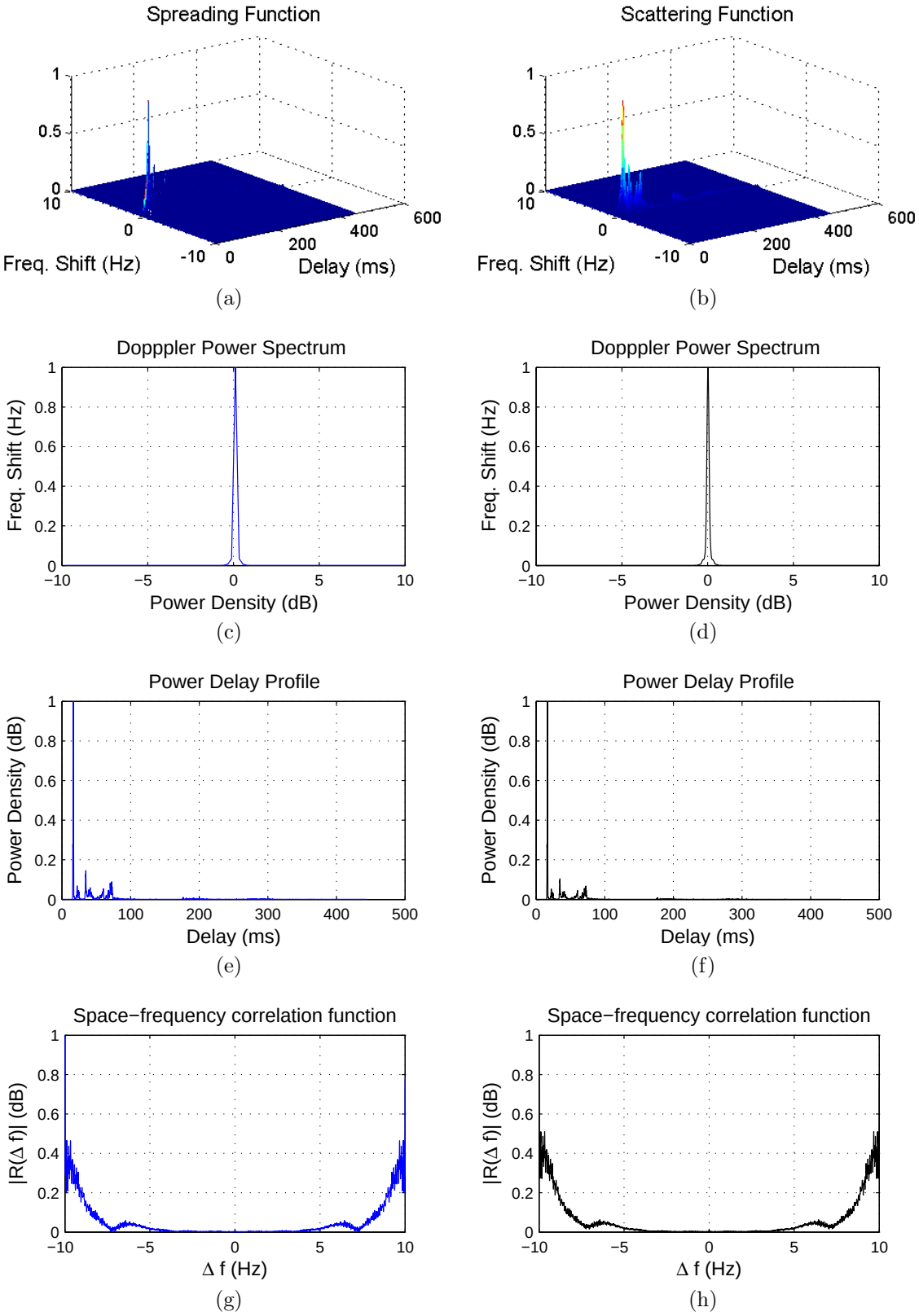

Figure 3: PRBS signal of length 1023: (a)3-D spreading function(b)3-D scattering function (c) Doppler power spectrum of a. (d) Doppler power spectrum of b.(e)Power delay profile of a. (f)Power delay profile of b. (g)Spaced frequency correlation function of e. (h)Spaced frequency correlation function of f.

LFM

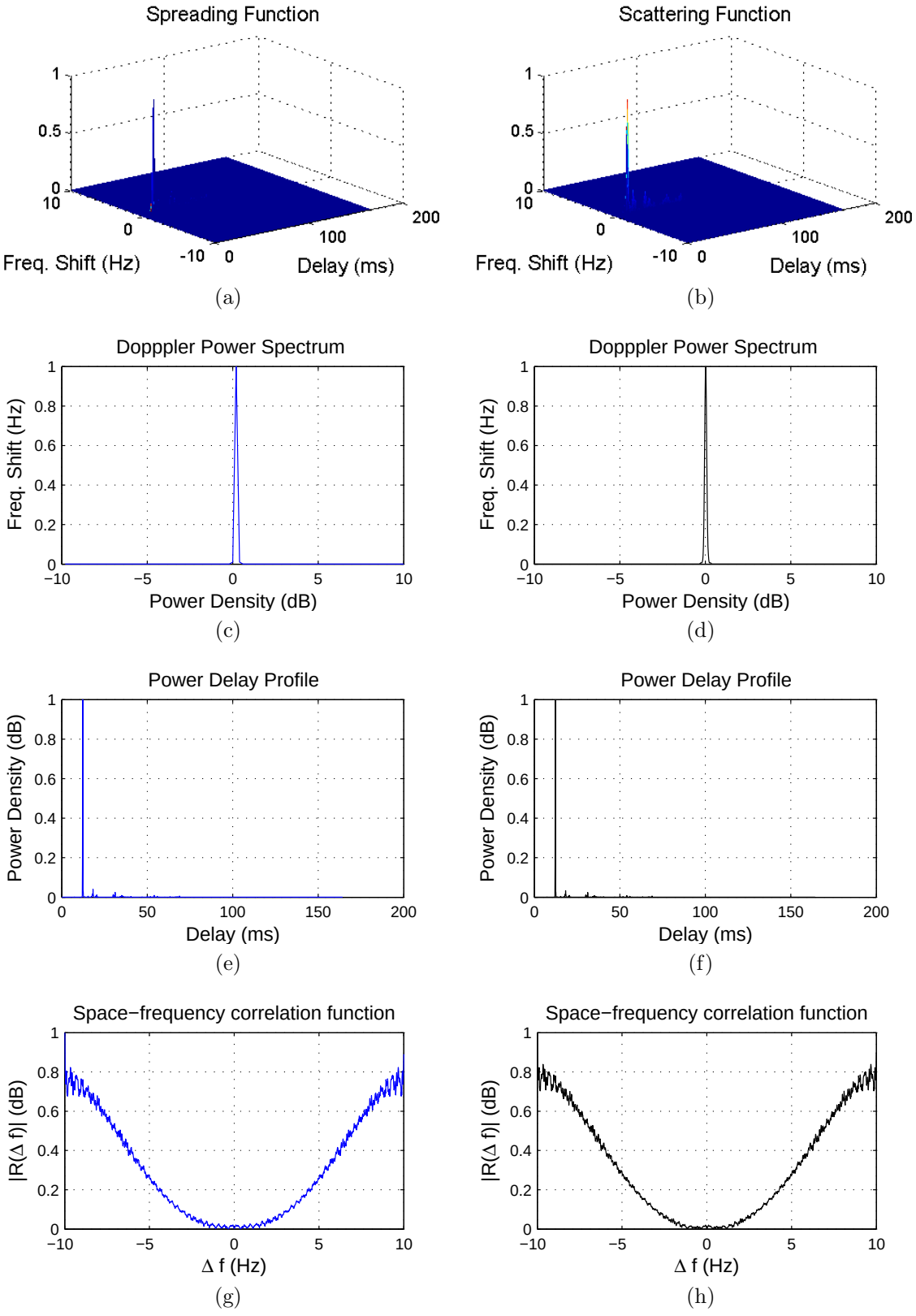

Figure 4: LFM signal : (a)3-D spreading function(b)3-D scattering function (c) Doppler power spectrum of a. (d) Doppler power spectrum of b.(e)Power delay profile of a. (f)Power delay profile of b. (g)Spaced frequency correlation function of e. (h)Spaced frequency correlation function of f.